The COMBO window: A chronic cranial implant for multiscale circuit interrogation in mice

Bradley Jay Edelman[*,#,1,2,3,4], Dominique Siegenthaler[*,1,3,4], Paulina Wanken[1,3,4], Bethan Jenkins[4,5,6], Bianca Schmid[2], Andrea Ressle[2], Nadine Gogolla[2], Thomas Frank[4,5,6], Emilie Macé[#,1,3,6]

[1] Brain-Wide Circuits for Behavior Research Group, Max Planck Institute for Biological Intelligence, Am Klopferspitz 18, 82152 Planegg, Germany

[2] Emotion Research Department, Max Planck Institute of Psychiatry, Kraepelinstrasse 2-10, 80804 Munich, Germany

[3] Department of Ophthalmology, University Medical Center, Göttingen, Robert-Koch-Strasse 40, 37075 Göttingen

[4] Cluster of Excellence "Multiscale Bioimaging: from Molecular Machines to Networks of Excitable Cells" (MBExC), University of Göttingen, Germany

[5] Olfactory Memory Research Group, Max Planck Institute for Biological Intelligence, Am Klopferspitz 18, 82152 Planegg, Germany

[6] Olfactory Memory and Behavior Research Group, European Neuroscience Institute and Faculty for Biology and Psychology, University of Göttingen, Grisebachstr. 5, 37077 Göttingen, Germany

*These authors contributed equally to this work
Correspondence to: bradley_edelman@psych.mpg.de, emilie.mace@bi.mpg.de

ABSTRACT:

Neuroscientists studying the neural correlates of mouse behavior often lack access to the brain-wide activity patterns elicited during a specific task of interest. Fortunately, large-scale imaging is becoming increasingly accessible thanks to modalities such as Ca^{2+} imaging and functional ultrasound (fUS). However, these and other techniques often involve challenging cranial window procedures, and are difficult to combine with other neuroscience tools. We address this need with an open-source 3D-printable cranial implant - the COMBO (**C**hr**O**nic **M**ultimodal imaging and **B**ehavioral **O**bservation) window. The COMBO window enables chronic imaging of large portions of the brain in head-fixed mice while preserving orofacial movements. We validate the COMBO window stability using both brain-wide fUS and multi-site two-photon imaging. Moreover, we demonstrate how the COMBO window facilitates the combination of optogenetics, fUS and electrophysiology in the same animals to study the effects of circuit perturbations at both the brain-wide and single-neuron level. Overall, the COMBO window provides a versatile solution for performing multimodal brain recordings in head-fixed mice.

INTRODUCTION:

Acquiring large neural activity datasets from distant and interconnected regions is paramount to understanding the neural correlates of behavior [1,2]. For animal models with small brains, such as zebrafish and fruit flies, optical imaging approaches can fulfill this need by acquiring whole-brain activity during behavior at cellular resolution [3,4]. By contrast, in the larger mouse brain no such optimal technique is currently available. Large-scale recording modalities such as functional MRI (fMRI), wide-field Ca^{2+} imaging and more recently fUS imaging exhibit a relatively low spatio-temporal resolution. On the other hand, techniques with cellular resolution such as two-photon microscopy and electrophysiology suffer from limited brain coverage. Therefore, as no single modality is capable of imaging whole-brain activity in mice at the level of individual neurons, alternative strategies using existing tools must be employed. One recent strategy is to utilize techniques with low brain coverage (e.g. Neuropixel recordings) in a highly parallelized manner to acquire large quantities of neuronal recordings across different regions of the brain during the same standardized behavioral task [5–7]. An alternative strategy that is more suitable to non-standardized behaviors is to combine different modalities such that information from multiple spatio-temporal scales is acquired in the same animals. In this case, large-scale recordings can inform which individual regions should be investigated in more detail without a priori knowledge [8]. Beyond acquiring neural data, it is increasingly popular to manipulate specific circuits (e.g. optogenetics) to determine their causal impact on behavior. Combining optogenetics and large-scale imaging is a powerful approach to identify unexpected regions modulated by specific manipulations and to guide targeted recordings [9]. However, combining all these techniques in a single animal is technically challenging and therefore relatively rare.

A common feature of some of the most popular techniques used in neuroscience (electrophysiology, wide-field imaging, two-photon microscopy, optogenetics, fUS) is that they are

most often applied through a cranial window. This is either because direct access to the brain is needed, e.g. for electrode or fiber implantation (electrophysiology, optogenetics, fiber photometry), or to maximize imaging quality and depth (optical imaging, fUS) [10–12]. Early chronic cranial windows developed specifically for optical imaging reported clear optical access to the brain at cellular resolution for months at a time [13,14]. However, these windows utilize flat glass coverslips that can cause anatomical distortions when placed over large areas of curved tissue. Therefore, such approaches are limited in spatial extent, often covering only 2-5 mm^2 of the brain [15]. A solution to this problem was provided by the "Crystal Skull" implant, a curved glass coverslip giving access to 75 mm^2 of the dorsal cortex, which is commonly used for wide-field imaging [16]. However, glass windows are not compatible with methods such as electrophysiology and fUS. Recently, this restriction has been largely overcome with other geometry-based approaches that involve shaping a plastic film to the curvature of the skull and brain [17,18]. Such examples are also accompanied by curved implant frames that can be easily attached to the skull and combined with a lightweight head-plate for head-fixation under an imaging apparatus [17,18]. In particular, the "See-Shell" implant designed by Ghanbari et al. [18] provides access to 45 mm^2 of the dorsal cortical surface and can be 3D-printed/laser cut using low-cost machines often found in laboratory settings. Such window designs exhibit robust long-term functionality, minimize the impact on brain tissue, and suggest a standardized surgical procedure. Despite these advantages, such designs have not been tested for acoustic imaging and are still limited in field of view. In parallel, other implants have been proposed to specifically accommodate fUS while being compatible with optical methods [19–21]. However, these implants are designed primarily for single-slice fUS acquisitions and therefore exhibit limited coverage, whereas volumetric fUS can now acquire a much larger portion of the mouse brain in a single acquisition (~ 1 cm^3) [22].

Here we propose to simplify multimodal imaging across spatial-temporal scales in head-fixed behaving mice using a chronic cranial implant, termed the COMBO window. The COMBO window aims to address unresolved issues with currently available cranial window implants by providing a larger field of view and compatibility with optical and acoustic imaging, as well as with local recording and manipulation methods. Importantly, the COMBO window was specifically designed to also preserve head-fixed behaviors and to ensure unobstructed facial access for videographic recordings. We first validated modality-specific versions of the COMBO window for awake imaging with both fUS and two-photon Ca^{2+} imaging. We then further validated an additional variant of the COMBO window with the combination of fUS, optogenetics, behavioral analyses and electrophysiology in the same animals. To increase accessibility, we developed all components of the COMBO window and head fixation components for 3D printer or laser cutter production, and provide all relevant files (**Supplementary Files 1-14, 10.5281/zenodo.8223630).** By doing so, the most appropriate off-the-shelf option can be used for individual applications and can be 3D-printed in-house without the need for significant customization. Overall, the COMBO window provides a unified solution to the requirements of a large variety of neuroscientific experiments that benefit from access to a large portion of the mouse brain during behavioral tasks.

RESULTS:

Design principles of the COMBO window

The COMBO window consists of three parts: a resin-based implant frame, a metallic head-plate, and a protective transparent film (**Figure 1a, Supplementary Figure 1**). We chose an asymmetric design to facilitate unobstructed videography of the animals' full face and body during head-fixed experiments. To achieve high stability and durability of the COMBO window, we fit the core structure closely to the surface of a standard mouse skull [18] (**Figure 1a**). A central hole provides access to an area of ~ 90 mm^2 of the dorsal skull, spanning from just posterior to the olfactory bulbs to the cerebellum in the anterior-posterior axis (**Figure 1b,c**). Thus, the majority of the cerebral cortex, striatum, pallidum, hippocampus, thalamus, hypothalamus, and midbrain can be accessed through this opening (**Figure 1c**). Flat protrusions with screw holes extending from the side and rear of the COMBO window, as well as a notch at the front of it, act as attachment points for the head-plate. The COMBO window is sealed with a 125 µm thick polymethylpentene (PMP) film, which is slightly arched using a 3D-printed mold (**Supplementary File 14**) that mimics the curvature of the skull (**Supplementary Figure 2a**). This ensures that the distance between the brain surface and the film is constant across the entire cranial window. Similar thermoplastic polymers of various thicknesses can also be used [11,18], however we have found that 125 µm PMP offers an optimal compromise between flexibility and durability. We provide detailed schematics and instructions for the preparation and installation of the COMBO window, as well as for the cranial window surgery itself (**Appendix 1, Supplementary Figure 2**), to encourage optimal and consistent use. For additional reference, details regarding cranial window surgery and the challenges associated with large skull openings have been described elsewhere [23,24].

Furthermore, to enable the widespread use of the COMBO window across labs and to provide a unified solution for multiple experimental needs, we provide numerous versions (**Figure 1d)** that are all compatible with our custom-designed head-plate and head-plate holder (**Figure 1e**). First, to facilitate whole-brain fUS recordings, we added an upward protruding ring from the surface of the implant frame to contain the ultrasound gel during extended imaging sessions. For this reason, we termed this the "cup" version and it is intended for fUS applications. Second, to make the COMBO window compatible with optical modalities such as two-photon Ca^{2+} imaging, we created a "flat" version without the cup to accommodate the limited working distance of typical high numerical aperture objectives used in two-photon imaging (note that fUS can also be performed through the flat version). Third, to complement these two standard versions, we designed additional variations compatible with circuit manipulation techniques that require a physically implanted object such as an optical fiber or electrode (**Figure 1d**). As recording and stimulation sites vary depending on the scientific question, we created seven variations with different implantation compartments that accommodate different target regions without the need for additional modifications. While these compartments reduce the maximum cranial window size, such variations still provide access to an opening of between 50 and 80 mm^2 of the dorsal skull. 3D-printable files (.stl) for all versions of the COMBO window are provided in **Supplementary Files 1-7**, a laser-cutter file for the universal head-plate (.dwg) in **Supplementary File 10**, and

various files for the head-plate holder in **Supplementary Files 11-13**. All files are additionally provided at an open-source repository for free public download (**10.5281/zenodo.8223630**).

To verify the long-term biocompatibility of the COMBO window, we immunohistochemically examined brain slices six weeks after implantation by visualizing reactive gliosis through glial fibrillary acidic protein (GFAP), a widely used marker for astrocytes and the immune response of the brain [25]. Overall, we found that chronic exposure to the COMBO window did not elicit a widespread inflammatory response in the cortex (**Figure 1f-e**). However, we anecdotally observed small and sparsely distributed patches of increased GFAP signal in implanted animals (**Supplementary Figure 3a-b**) that were likely caused by localized surgical damage rather than chronic inflammation. In fact, an unbiased quantification of GFAP fluorescence in 18 superficial and uniformly distributed cortical regions-of-interest in each animal revealed no significant difference between those implanted with the COMBO window (N = 6, six weeks post-installation) and those without (N = 5) (**Figure 1f-e**). These results demonstrate that our design provides access to a large fraction of the mouse brain without causing long-lasting inflammation.

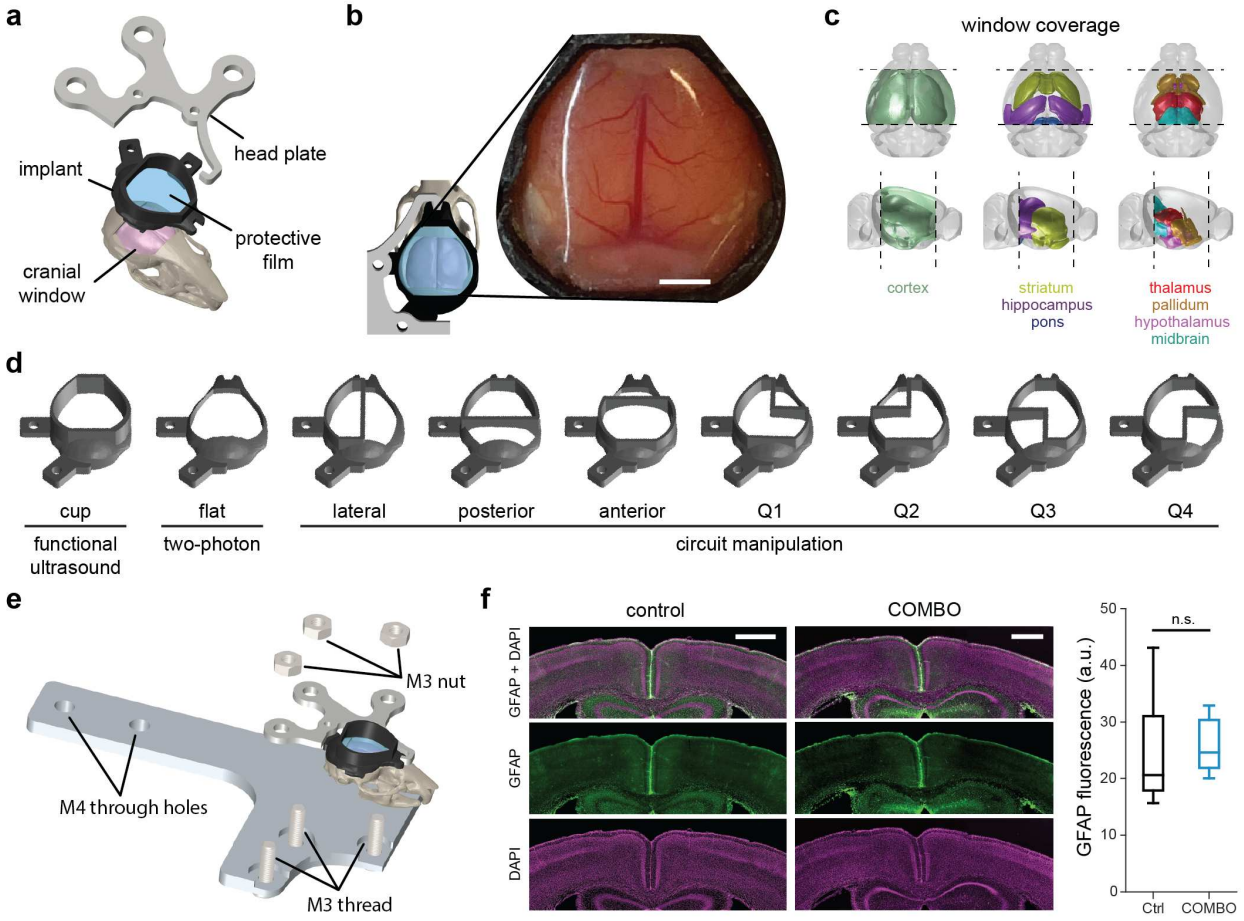

Figure 1: Design principles of the COMBO window

a Computer aided design (CAD) of the COMBO window and corresponding head-plate. The core shape of the implant was fitted to the surface of a standard mouse skull, sealed with a protective

film and accompanied by a standard head-plate. **b** Top-view of the implant CAD design. An example image of a whole-brain cranial window and the COMBO window installed on a mouse four weeks after surgery. Scale bar represents 2 mm. **c** 3D diagrams displaying the estimated window coverage, which includes the cerebral cortex, striatum, hippocampus, thalamus, hypothalamus, pallidum, midbrain, and pons. **d** Two whole-brain implant designs optimized for functional ultrasound imaging ("cup") and two-photon fluorescence microscopy ("flat"). Seven additional designs (with a cup) were created to accommodate a chronic implant for circuit manipulations or recordings. **e** CAD design of the standard head-plate holder that provides stable head fixation for the COMBO window. **f** Glial fibrillary acidic protein (GFAP) fluorescence in the cortex (bregma -1.0 mm AP) of a representative animal with (left) and without (right) the COMBO window. Images show the GFAP + DAPI (top), GFAP (middle) and DAPI (bottom) signal. Scale bars represent 500 μm. There was no significant difference in cortex-wide GFAP immunofluorescence between animals without (N = 5, black) and with the COMBO window (N = 6, blue). Boxplots represent the median (center line), 25th and 75th percentiles (lower and upper box), and the 1st and 99th percentile (whiskers). One-way repeated measures ANOVA on ranks. Main effect of the COMBO window: n.s. $p > 0.05$.

The COMBO window preserves freely moving behavior and facial expressions

We next characterized the impact of the COMBO window on various aspects of mouse behavior. Behavioral effects due to the weight of the implant may not be apparent in head-fixed experiments, but could significantly affect an animal's wellbeing [26]. Therefore, we assessed the effects of head-plate weight on natural behavior during an open-field free foraging task (**Figure 2a**) [27]. For these experiments, we implanted wild-type C57BL/6 mice (N = 7) with the "cup" version of the COMBO window and attached a 1.5 mm thick stainless steel head plate (2.5 g) as an upper bound of added weight. Two weeks after head-plate attachment, the mice were left to explore a 40 cm x 40 cm arena containing randomly placed food pellets for 10 minutes while their movement was tracked. We compared different locomotion-related variables between implanted (N = 7) and control mice (N = 7): all statistical tests and results are provided in **Supplementary Table 1**. We did not find any observable difference in open field coverage or cumulative distance traveled between the two groups of animals (**Figure 2b-c**). More specifically, there was no significant difference in the total distance traveled or locomotor speed (**Figure 2d-e, Supplementary Table 1**). We further assessed whether the unilateral head-plate design and unbalanced weight distribution impaired the animals' ability to turn by measuring the tortuosity of their open field trajectory. The tortuosity was not significantly different between control and implanted mice (**Figure 2f, Supplementary Table 1**). Considering that female mice typically weigh less than male counterparts, we further inspected sex-dependent differences across the same parameters. We found a significant effect of sex on total distance and speed (**Supplementary Figure 4a-c, Supplementary Table 1**), however, no difference between implanted and control mice within a sex, indicating that these open field observations generalize to both male and female mice.

In addition to naturalistic behavior, we also sought to determine the effects of the implant on orofacial movements as the implant reaches the lateral-most edges of the skull and could

impact the nearby skin and muscles. In recent years, head-fixed neural recordings have been commonly accompanied by the analysis of concurrent orofacial videography to link brain activity with the detailed assessment of behavioral states [28–30]. To verify that orofacial movements are preserved with the COMBO window, we tested the ability to identify facial readouts of emotion states which rely on stereotyped position patterns of the ears, snout, and whiskers [31]. We implanted wild-type C57BL/6 mice (N = 3) with the COMBO window and subsequently habituated them to head-fixation on a running wheel. Mice were then provided with individual trials of sucrose and quinine in subsequent runs to elicit the emotions of pleasure and disgust, respectively (**Figure 2g**). These two stimulus-emotion pairings were chosen since the associated facial expressions comprise movements that span the full range-of-motion of the ears and snout. When examining the videographic frames identified as prototypical emotion states, (see Methods for details) we observed in all three mice the stereotypical features of the two facial expressions (**Figure 2h**, **Supplementary Videos 1 - 2, Supplementary Figure 4d**). As originally reported in mice with no cranial window [31], we found that the readout of pleasure and disgust, quantified as the temporal correlation with a prototypical facial expression of emotion, were highly selective for sucrose and quinine, respectively (**Figure 2i-j**). The disgust response during quinine trials was significantly larger than that during baseline, whereas it was non-existent during sucrose trials (**Supplementary Table 2**). Accordingly, the pleasure response during sucrose trials was significantly larger than that during baseline trials, but was absent in quinine trials (**Supplementary Table 2**), demonstrating successful emotion identification from the orofacial movements of implanted animals. Overall, these results show that the COMBO window does not affect locomotor or orofacial behavioral readouts in freely moving or head-fixed contexts, respectively.

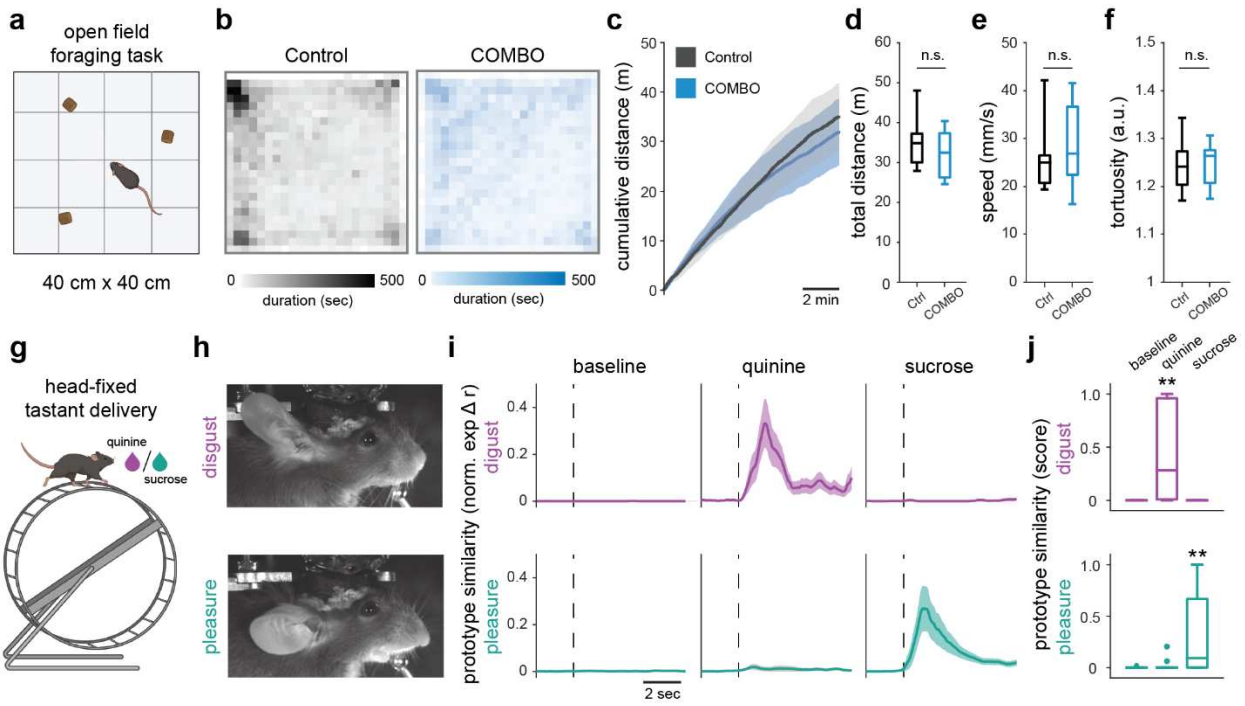

Figure 2: The COMBO window preserves freely-moving behavior and facial expressions
a Animals with a COMBO window (COMBO) (N = 7) and control (ctrl) (N = 7) performed an open field foraging task to test the effect of the implant and head plate on freely moving behavior. **b** Average trajectories of control mice (left, gray) and mice with a "cup" implant and 1.5 mm stainless steel head plate installed (right, blue) running in a 40 x 40 cm open field for 10 min. **c** Cumulative distance of the control and COMBO mice over the course of 10 min runs. **d-f** The total distance (**d**), median speed during running (**e**), and tortuosity during exploration (**f**) of control and COMBO mice. In all plots black color represents control mice and blue color represents COMBO mice. **g** Head-fixed mice (N = 3) were administered five trials of sucrose and quinine (2 sec each) in separate runs to extract and evaluate the specificity of the pleasure and disgust facial readouts of emotions. **h** Individual videographic frames displaying a prototypical disgust and pleasure facial expression from a representative mouse with the "cup" version of the COMBO window. **i** Time-resolved normalized pleasure and disgust facial prototype similarity scores during baseline, sucrose and quinine events (n = 15 trials each). Dark lines and light shaded areas represent the mean ± s.e.m. across trials. **j** Trial-based normalized prototype similarity scores during baseline, sucrose and quinine trials (n = 15 trials). Boxplots represent the median (center line), 25th and 75th percentiles (lower and upper box), and the 1st and 99th percentile (whiskers). Two-way ANOVA on ranks with main effects of sex and COMBO window. Main effect of the COMBO window (N = 7 per group): n.s. $p > 0.05$. Wilcoxon rank sum test between tastant and baseline events: ** $p < 0.01$.

Brain-wide fUS imaging through the COMBO window

We next aimed to demonstrate the utility of the COMBO window for volumetric brain-wide fUS imaging [22]. fUS imaging measures blood volume as a proxy of brain activity [32] and, in the context of multimodal imaging, gives access to large-scale information while being compatible

with standard behavior rigs. We chose to use visual stimulation because the mouse visual pathway has been previously described in detail using both fUS and other large-scale imaging techniques [8,33]. We implanted wild-type C57BL/6 mice (N = 5) with the "cup" version of the COMBO window before habituating them to a head-fixed context in which the mouse is resting in a tube in front of a display screen (**Figure 3a**). At 4-6 weeks after implantation we acquired brain-wide fUS data while simultaneously presenting awake mice with drifting gratings moving along the four cardinal directions in the binocular visual field (**Figure 3a, Supplementary Video 3**). This visual stimulus specifically triggers oculomotor movements in awake mice [8]. Each stimulus block (12 seconds on, 12 seconds off) was presented 3 times in a randomized order for a total recording time of less than 5 min per session. Using an ultrasound transducer specific to volumetric acquisition (called a "matrix probe") we acquired volumetric fUS brain data at 2 Hz temporal resolution [22]. We examined the hemodynamic response in core visual areas such as the primary visual cortex (VIS), lateral geniculate nucleus (LGN) and superior colliculus (SC). As expected, the fUS signal within these regions correlated with the visual block stimulus (r_{VIS} = 0.68, r_{SC} = 0.71) (**Figure 3b**). We then assessed the brain-wide, voxel-wise responses using a general linear model analysis. We observed significant bilateral activity in hubs of the visual system, including the VIS, SC and LGN (**Figure 3c-d**). The symmetry indicates that the unilateral design of the COMBO window does not obstruct the perception of bilateral visual inputs. Additionally, as previously reported, we observed a decrease in amygdala activity (**Figure 3c-d**) due to the oculomotor movements elicited by the drifting gratings [8]. Lastly, a substantial increase in activity was found in the dorsal-medial striatum (DMS), the visual domain of the striatum [34], as well as the anterior cingulate cortex (ACC) (**Figure 3c-d**). The activation in these anterior regions further refines the characterization of brain-wide visual responses to these stimuli, which had not been observed in previous work due to a smaller and more posterior field of view [8]. The ability to detect visual-evoked activity in brain regions spanning more than 5,4 mm in the anterior-posterior direction and 8,4 mm in the medial-lateral direction highlights the utility of an implant that can accommodate such a large cranial window.

Imaging experiments in awake animals come with the advantage of enabling brain activity measurements during a large repertoire of natural behaviors. By contrast, imaging under anesthesia can improve data quality due to reduced animal movement and fewer motion-induced artifacts. Moreover, the investigation of sensory brain networks in anesthetized recordings is not confounded by neuronal activity elicited by ongoing behaviors. To compare the two approaches, we repeated the experiment in anesthetized mice (N = 4) using an identical visual stimulation paradigm. In this case, we expected a robust activation of the main visual pathway but no activation of the oculomotor-related pathways. Indeed, in anesthetized animals we also observed robust evoked activity in the core visual regions (**Figure 3c-d**), such as VIS, SC and LGN, with a similar evoked amplitude as in awake animals (**Figure 3b, d-e and Figure S5a**). We also observed that a cluster of regions, including the ACC and subregions of the amygdalar complex, were modulated by visual stimulation in awake, but not anesthetized animals (**Figure 3c, e, circles along vertical line**). Lastly, to demonstrate the durability of the COMBO window, we also collected brain-wide fUS data at two months post-implantation (n = 8 sessions) and still detected robust activation in the core regions of the visual system (**Figure S5c**). Due to animal license limitations, mice were sacrificed after this time point, however, the windows remained acoustically

viable. Together, these results demonstrate that the COMBO window enables longitudinal and stable brain-wide fUS imaging in behaving mice.

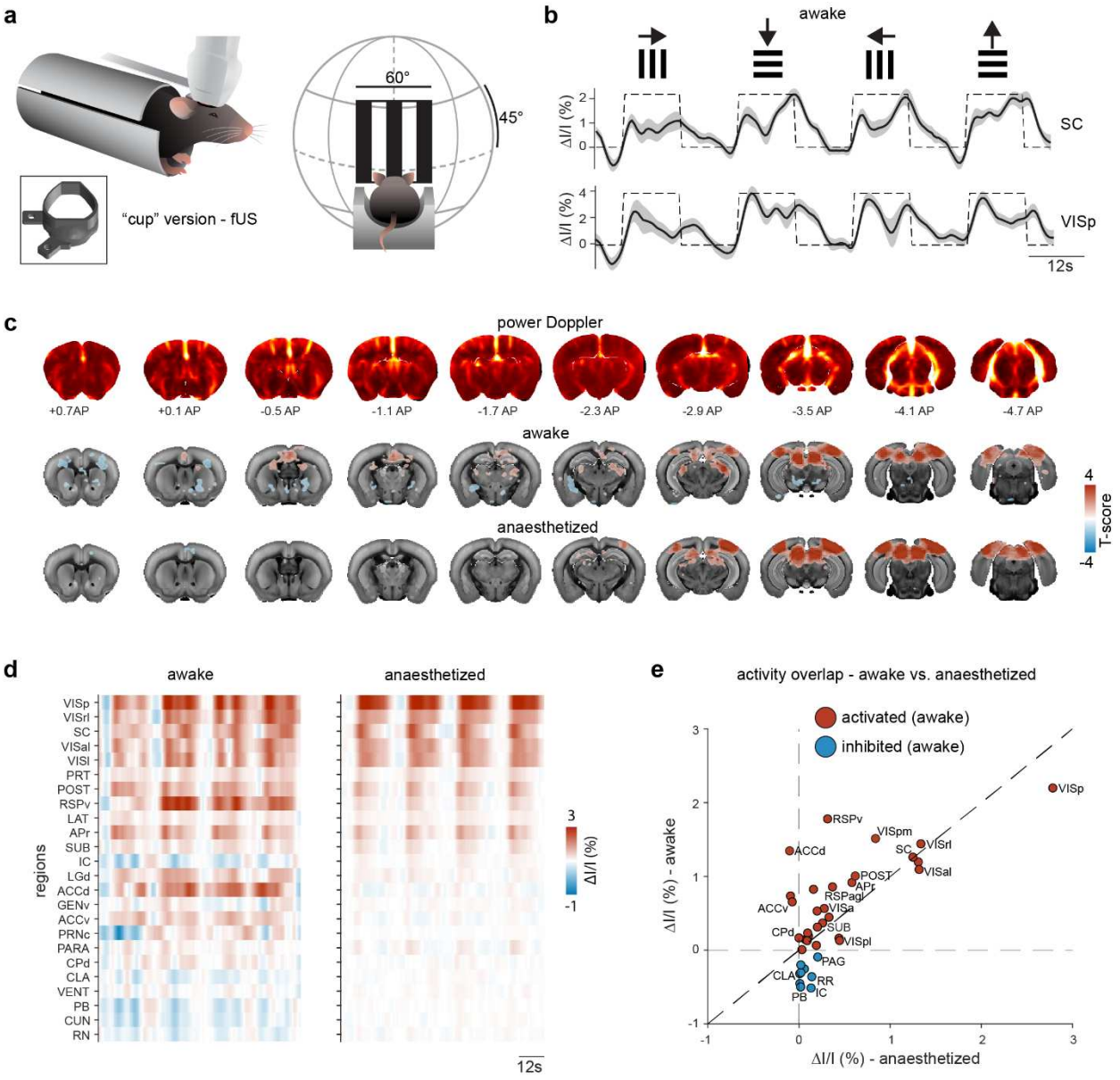

Figure 3: Awake brain-wide imaging through the COMBO window

a Schematic representation of fUS imaging in mice in a holding tube with the "cup" version of the COMBO window. Awake mice were presented with drifting gratings in the upper visual field (size 60° visual angle) while brain-wide fUS data was collected. **b** Evoked fUS signals were observed in the primary visual cortex (VIS) and superior colliculus (SC) in response to drifting gratings moving in all four cardinal directions. The dashed black line indicates the stimulus timing. The dark black line and light gray shaded area represent the mean ± s.e.m. across sessions (N = 4 mice, n = 46 sessions). **c** Coronal slices of power Doppler images (top row) and T-maps (middle row: awake, bottom row: anesthetized) are overlaid on the Allen Brain Atlas at the indicated

positions (anterior-posterior distance from bregma). Voxels with a significant T-score across sessions ($p < 0.05$, FDR-corrected) are displayed in color (awake: N = 4 mice, n = 46 sessions, anesthetized: N = 5 mice, n = 32 sessions). **d** fUS data was segmented into anatomical brain regions. Only regions that were significantly modulated by the visual stimulus in the awake state are displayed (correlation coefficient significantly different from zero across sessions, $p < 0.05$, FDR-corrected). **e** The mean fUS signal ($\Delta I/I$) in each region (same as **d**) during stimulus presentation plotted as the anesthetized (x-axis) vs awake (y-axis) state. Not every region label is shown for visualization purposes. Regions are colored according to the fUS signal in the awake state (blue circles for negative $\Delta I/I$, red circles for positive $\Delta I/I$).

The COMBO window enables multisite two-photon imaging during behavior

To assess the ability to capture single-cell activity through the COMBO window using optical imaging techniques, we created the "flat" version by removing the upward protruding cup, which allows closer positioning of the objective towards the brain surface (working distance of objective: 2 mm). In cases where longitudinal and multimodal imaging is preferred, the "flat" COMBO window can also be used with fUS imaging, as the "cup" simply helps to contain the ultrasound gel. The COMBO window was installed on mice (N = 3) expressing the genetically encoded Ca^{2+} indicator GCaMP6s [35] in cortical excitatory cells. At 10 weeks post-implantation we leveraged the large cranial window by imaging Ca^{2+} signals at a depth of 200-300 μm (layer 2/3) in the secondary motor (M2) and retrosplenial (RSC) cortices, two brain areas located at the anterior and posterior edges of the cranial window (**Figure 4**). Across these mice, we recorded Ca^{2+} signals from a total of 150 neurons in M2 and 180 neurons in RSC. During two-photon imaging the animals were head-fixed on a running wheel and spontaneous movements were captured using videographic recordings (**Figure 4a**). To directly assess the stability and suitability of the COMBO window for two-photon recordings during behavior, we examined pre- and post-registration metrics via the *Suite2p* processing framework [36]. As seen in similar experimental setups [37,38], we observed larger frame-wise displacements in both the x and y directions during periods of increased locomotion (**Figure 4b**). To measure the ability to successfully recover cellular traces, we examined the residual drift of the spatial principal components extracted by *Suite2p* after non-rigid registration. The residual drift value for both the M2 (n = 8 runs, median = 0.27 μm, IQR [0.23, 0.49]) and RSC (n = 7 runs, median = 0.10 μm, IQR [0.03, 0.12]) recordings was well below 1 μm (**Figure 4c**), and is similar to the values reported by recently benchmarked two-photon imaging studies [27,36]. This shows that the COMBO window provides sufficient stability for high-resolution two-photon imaging across distributed cortical areas in behaving animals.

While the previous analysis demonstrates stability from a data analytical standpoint, we further ensured that the COMBO window enables the acquisition of neural activity associated with head-fixed mouse behavior. For this, we took advantage of a simple but robust phenomenon whereby a significant portion of neural activity in the mouse cortex can be explained by behavioral variables such as locomotion [29,39]. Specifically, we performed keypoint tracking of the forepaws from videographic recordings (see methods for details), and compared a time-resolved output of locomotion to neuronal traces in both M2 and RSC (**Figure 4d-e**, **Supplementary Video 4**). As demonstrated in various large-scale two-photon studies, we found that the first principal

component (PC) of population activity was highly correlated (Pearson correlation coefficient) with locomotion in both M2 (n = 8 runs, median r = 0.70, IQR [0.27, 0.79]) and RSC (n = 7 runs, median r = 0.55, IQR [0.28 0.71]). Similarly, at the individual neuron level, we found that the majority of cells were significantly correlated ($p < 0.001$) with locomotion in both recording sites (84% in M2, 85% in RSC, **Figure 4e-f**). More specifically, we observed a positive correlation with locomotion for the majority of M2 cells (positive: 61%, negative: 23%), while positively and negatively correlated cells represented a similar proportion of all neurons in RSC (positive: 41%, negative: 44%) (**Figure 4f**)**.** Nevertheless, in both regions a small fraction of cells was neither positively or negatively linked to locomotion (16% in M2, 15% in RSC). Together these results demonstrate the utility of the COMBO window for optical imaging at cellular resolution across the mouse cortex during head-fixed behavior.

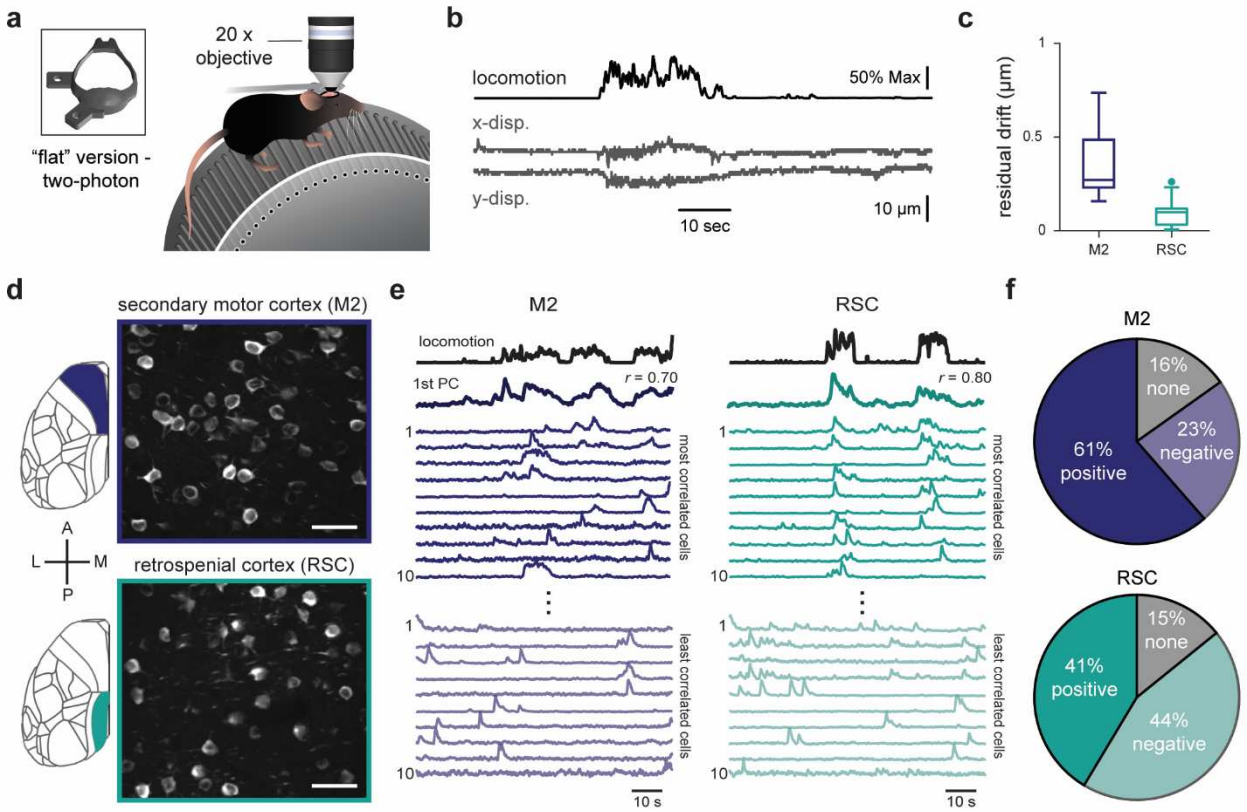

Figure 4: The COMBO window enables multisite two-photon imaging during behavior
a Schematic of two-photon Ca^{2+} imaging in mice on a running wheel with a "flat" version of the COMBO window. **b** Example locomotion trace along with the framewise displacement of images in the x and y direction during a representative 90 sec recordings session. **c** Residual drift of secondary motor cortex (M2) (n = 8 recordings) and retrosplenial cortex (RSC) (n = 7 recordings) recordings after non-rigid registration of the images. Boxplots represent the median (center line), 25th and 75th percentiles (lower and upper box), and the 1st and 99th percentile (whiskers). **d** Representative maximum intensity projection of a 90 sec recording acquired 200-300 µm below the pial surface in M2 (top, purple) and RSC (bottom, blue). Scale bars represent 50 µm. **e** Example 90 sec recording from the M2 (left) and RSC (right), showing the first principal component of the neuronal population activity (dark red) as well as the times series from the ten

cells most (light red) and least (light blue) correlated with locomotion. **f** Pie charts representing the proportion of individual cells significantly correlated with locomotion in M2 (150 cells, N = 3 mice, n = 7 recordings) and RSC (180 cells, N = 3 mice, n = 7 recordings). P-values for each cell-locomotion correlation combination were FDR-corrected and thresholded at $p < 0.001$. Remaining cells were then categorized as positive (light red) or negative (light blue) based on the sign of the correlation. Cells with a p-value > 0.001 were categorized as none (gray).

Multimodal investigation of optogenetic circuit perturbations

Optogenetic approaches are powerful tools to manipulate genetically identified cell types or brain regions. We aimed to create a framework that enables the identification of brain-wide activity patterns in response to specific optogenetic activation or silencing in behaving animals, as well as the subsequent verification of these patterns using alternative invasive techniques such as electrophysiology in the same animals. Longitudinal studies that enable within-animal verification are particularly useful for optogenetics, which can exhibit high variability in opsin expression. To increase the flexibility of this framework, we designed seven additional versions of the COMBO window to provide different “off-the-shelf” options for different experimental needs (**Figure 1d**). For validation of this design principle in awake animals, we targeted M2, as optogenetic activation of this region has been previously shown to cause a robust increase in locomotion [40]. We bilaterally injected an adeno-associated virus carrying the channelrhodopsin-2 (ChR2) construct under the *Camk2a* promoter (AAV-CaMKIIa-ChR2-EYFP) into M2 in wild-type C57BL/6 mice (N = 4). In addition, optic fibers were implanted at an angle and a cranial window was installed, all of which were encapsulated and stabilized using the “anterior” version of the COMBO window (**Figure 5a-b**). Transduction was verified at the end of the experiment using immunohistochemistry, which confirmed strong expression of ChR2-EYFP in the bilateral M2 (**Figure 5b).** We first analyzed behavioral responses elicited by optogenetic activation of M2 using motion energy analysis of simultaneously acquired videographic recordings (**Figure S6a**). As expected, 10 seconds of blue light at 20 Hz elicited a robust increase in locomotion (peak z-score: 9.51 ± 2.17) (**Figure 5c-d**). This stimulation was also associated with an increase in whisking (peak z-score: 1.98 ± 0.46), a more detailed behavior that could be captured due to the unilateral design of the COMBO window (**Figure 5d and Figure S6b**).

In a subset of these animals (N = 2) we also simultaneously acquired volumetric fUS recordings to observe the brain-wide activity associated with optogenetic activation of M2. We found robust stimulation-locked activated voxels throughout the brain (**Figure 5e**). Specifically, we observed strong activation in the thalamus, the midbrain and posterior/medial subregions of the striatum (**Figure 5e-f, h and Figure S6c**). Qualitatively, we observed a good correspondence of the observed fUS activity with documented M2 axonal projection patterns described in literature [41] as well as in the Allen Brain Connectivity Atlas (**Figure S6d**) [42]. To better understand the extent by which the observed brain activation patterns are driven by optogenetically-elicited behaviors, we exploited the natural variability of the recorded behavioral responses. More precisely, we identified trials that elicited strong bouts of locomotion and others that did not (see methods for threshold definition). By doing so, we compared the fUS activity during optogenetic stimulation in

the presence and absence of locomotion. Overall, we found that the fUS activation patterns were qualitatively similar between the two conditions (**Figure S6e**), suggesting that a large portion of the observed brain activity was a direct result of M2 stimulation and not an indirect consequence of the elicited behavior. These results together demonstrate that the COMBO window enables the observation of a large volume of the brain during bilateral optogenetic stimulation in behaving animals.

One additional advantage of using a polymer-based film to seal the implant, especially in contrast to glass coverslips, is the potential to directly access the brain using more invasive techniques. To demonstrate this feature, we acquired electrophysiological recordings in a subset of injected and implanted mice (N = 2) in response to optogenetic activation of M2. For this, we drilled small perforations in the film and lowered 32-channel silicon probes into the midbrain at coordinates where we previously observed strong fUS activation (AP: -4. mm, DV: -2.2 to -3.60 mm, ML: ±1.0 mm) (**Figure 5e, g-h**), and optogenetically activated M2 at 5 Hz (**Figure 5g-h**). We recorded 118 single units across the midbrain reticular nucleus and the motor-related superior colliculus (**Figure 5h-i**). In correspondence with our fUS results and the known M2 axonal projection patterns to the midbrain [41,42], we observed a strong increase in firing rate at the population level during M2 activation (peak z-score: 17.87 ± 3.58 z-scores, **Figure 5h**). In total, stimulation-induced modulation of the firing rate was observed in 86% of the recorded cells, verifying the local fUS signal (**Figure 5i** and **Figure S6f).** More specifically, 72% of cells responded with a short-latency increase in firing rate (**Figure 5j**, cell 1, **Figure S6f**), 9% with a decrease in firing rate (**Figure 5j**, cell 2, **Figure S6f**) and 6% with an increase in firing rate at the offset of stimulation (**Figure 5j**, cell 3, **Figure S6f**). Overall, this proof-of-concept experiment shows the compatibility of the COMBO window with electrophysiological recordings and highlights the overall versatility of the design.

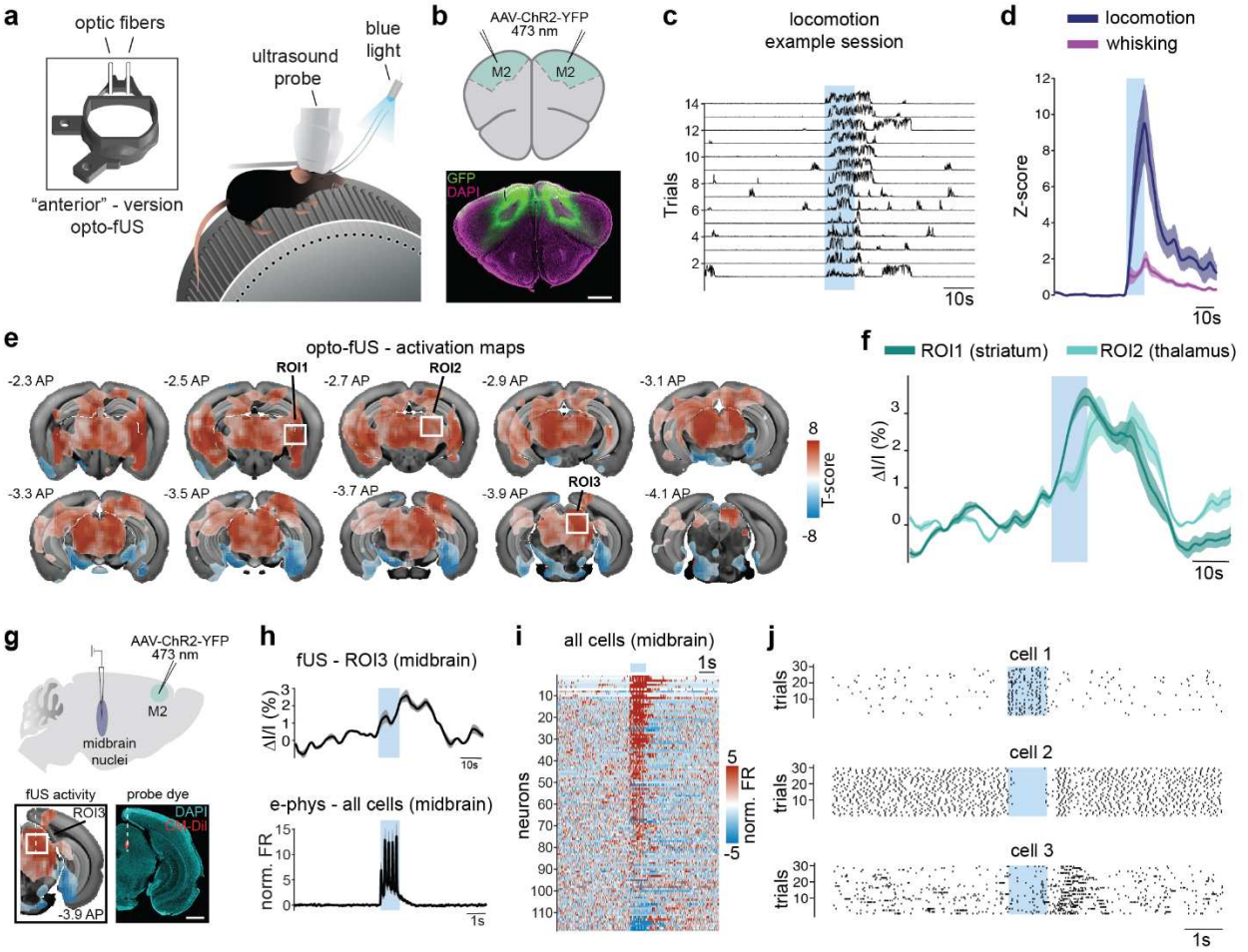

Figure 5: Multimodal investigation of optogenetic circuit perturbations

a Schematic representation of simultaneous fUS imaging and optogenetic stimulation (473 nm) of secondary motor cortex (M2) in mice with the "anterior" version of the COMBO window on a running wheel. **b** Before window implantation, AAV-CaMKIIa-ChR2-EYFP was injected bilaterally into M2, resulting in robust expression of ChR2-EYFP (EYFP in green, and DAPI in magenta). Scale bar represents 1 mm. **c-d** Behavioral parameters were assessed by quantifying motion energy changes from wheel and the whisker regions-of-interest (ROIs). **c** Consecutive trials from one session after applying a z-score transformation to the pre-stimulus baseline. Traces are rescaled between zero and one for visualization purposes. **d** Optogenetic activation of M2 results in a robust increase in locomotion and whisking (locomotion: 9.51 ± 2.17 peak z-score; whisking: 1.98 ± 0.46 peak z-scores (mean ± s.e.m.) (N = 4 mice, n = 18 sessions). **e** Average T-maps are overlaid on the Allen Brain Atlas at the indicated positions (AP distance from bregma). Voxels with a T-score significantly different from zero across sessions ($p < 0.05$, FDR corrected) are displayed in color (N = 2 mice, n = 12 sessions). White square boxes represent ROIs used to extract fUS time series data in **f** and **h**. **g** Electrophysiological recordings were performed during optogenetic stimulation of M2 to verify the fUS signal. Silicon probes successfully targeted the midbrain (CM-Dil dye in red and DAPI in cyan), where strong optogenetically-induced fUS activation was observed. Scale bar represents 1 mm. **h** The mean normalized firing rate across all recorded cells in the midbrain (bottom) compared to the average fUS signal (top) of ROI 3

(midbrain) from **e**. **i** The normalized firing rate of all recorded cells sorted by mean activity during optogenetic stimulation. **j** Raster plots showing all spikes from a given session for three example cells, highlighting the diversity of single-cell responses. For all panels, blue squares indicate the time of optogenetic stimulation. Solid lines and shaded areas represent the mean ± s.e.m. across sessions or cells.

DISCUSSION:

In this work, we present a whole-brain cranial window implant for the independent and combined application of fUS imaging, optical imaging, optogenetics, electrophysiology and behavioral observations in head-fixed mice. We show that the COMBO window is well tolerated by implanted animals and preserves both detailed orofacial movements (e.g. emotion readouts) and natural freely moving behavior. In separate cohorts, we demonstrated the feasibility of using fUS and optical imaging to obtain brain-wide (fUS) and single cell (two-photon) measurements of neural activity, respectively, through the COMBO window in behaving mice. Finally, we demonstrated that the COMBO window can be used to observe the brain-wide effects of optogenetic circuit manipulations in head-fixed mice. Importantly, the COMBO window allowed us to perform an array of different recordings and manipulations all in the same animals. For example, here we utilized the COMBO skull to simultaneously observe whole-brain activity patterns and elicited behaviors induced by targeted cell-type specific activation of M2, as well as the subsequent electrophysiological recordings in distant targeted brain regions. An open-source design and detailed protocols are provided to facilitate the adoption of the COMBO window by neuroscience labs (**Supplementary Files 1-14, Supplementary Figures 1-2, Appendix 1, 10.5281/zenodo.8223630)**.

The proof-of-concept experiments performed in this study were specifically designed to investigate the usability of the COMBO window, however, they also suggest new avenues for addressing a wide variety of future neuroscientific questions. First, we demonstrate that the COMBO window enables brain-wide imaging during behavior without any noticeable effects on mouse locomotion or orofacial movements. This unique advantage is further strengthened by the stability provided by the implant. For example, we observed consistent activation of the main visual pathways in both awake and anesthetized states. We also identified visually visual-evoked activity in the striatum and ACC in awake but not anesthetized mice, potentially reflecting a state-dependent recruitment of brain regions. This is in contrast to a similar comparison study performed using fMRI where a loss of apparent cortical activation was reported in the awake state compared to the anesthetized state [33]. This discrepancy may be due to differences in the mode of visual stimulation (drifting gratings vs flashing LED) or in the technical sensitivities between the two methods [20,43]. Overall, the acquisition of state-dependent and brain-wide activation patterns in awake animals, as we demonstrate with the COMBO window, enables the investigation of neuronal substrates underlying behavior. When paired with the preserved readouts of naturalistic behaviors, this framework suggests that the COMBO window can be used to study brain-states that extend beyond the sensory domain.

An important feature of COMBO is its utility for measuring brain activity at different spatio-temporal scales with different modalities. Importantly, this carries the advantage of enabling the conversion of many cross-sectional studies to longitudinal/paired designs, which can markedly help minimize the number of animals used and maximize statistical power [19,20,43]. Here, we specifically validated the COMBO skull for compatibility with a number of commonly used neuroscience tools, however, it can also likely be paired with additional techniques. Foremost, as we confirmed the optical transparency of the window using two-photon imaging, we assume that other optical imaging techniques such as wide-field calcium imaging are also compatible. Furthermore, similar to our proof-of-concept optogenetic stimulation experiment, other techniques requiring direct access to brain tissue, such as fiber photometry, microcannulas or brain temperature sensing can also be implemented. However, it should be noted that the implantation of items required for these techniques reduces the potential size of an accompanying cranial window. Compatibility with (f)MRI is also theoretically possible, similar to what has been previously shown with other preparations [20,44] when imaging before the implantation of the head-plate or by replacing it by a non-metallic version.

With large cranial openings, the concept of motion-induced artifacts becomes important as the surrounding skull usually stabilizes smaller windows. While our awake fUS data contained higher noise than anesthetized recordings, standard processing steps (see methods) revealed visual-evoked fUS activity in core visual brain regions. Similarly, optogenetic stimulation of M2 evoked expected patterns of activation that were confirmed at the neuronal level with electrophysiological recordings. In our awake two-photon recordings, we also observed increased framewise displacement during periods of locomotion, however, image stacks were easily recovered using standard registration procedures implemented in open-source analysis toolboxes [36]. As with any head-fixed experiment, habituation to head-fixation is an important step for animal comfort and for minimizing motion-related noise. As explained in our protocol (**Appendix 1**), we find that at least five days of habituation, increasing the duration of head-fixation each day, is sufficient for stable fUS or two-photon recordings using the COMBO window. In the future, a version of the COMBO window that allows for direct attachment of the imaging device (ultrasound probe, miniscope, etc.) to the head-plate [45,46] could further reduce the effects of movement on data quality. Such a version could also be integrated in freely-moving contexts and thereby expand the repertoire of behaviors that can be investigated. Nevertheless, the COMBO window provides a flexible, standardized and open-source solution to combine various neural recording and manipulation techniques in awake head-fixed mice.

MATERIALS AND METHODS:

Animals

Male and female C57BL/6 mice (8 weeks old) were used for all fUS and behavior experiments. For two-photon calcium imaging, we used male mice (8 weeks old) that expressed GCaMP6s in excitatory cortical neurons (B6.DBA-Tg(tetO-GCaMP6s)2Niell/J [Jax, 024742] x B6.Cg-Tg(Camk2a-tTA)1Mmay/DboJ [Jax, 007004]. All animals were group-housed in a 12-hour reversed light-dark cycle and were provided with standard diet and water *ad libitum*. All behavioral experiments were performed during the dark cycle. All animal procedures were performed in accordance with the institutional guidelines of the Max Planck Society and the local government (Regierung von Oberbayern).

COMBO window preparation

COMBO window frames were printed using a stereolithography 3D printer (FormLabs, Form 2) using black resin (FormLabs). Minimal supports were placed with a 0.5 mm touchpoint size to ensure sufficient printing stability and to facilitate easy detachment afterward. Remaining support material was manually filed down to a smooth surface. The head-plate attachment holes were threaded for M1.4 screws and 125 µm thick polymethylpentene (Goodfellow) film was attached to the interior ridge of the frame using a combination of cyanoacrylate glue (Pattex) and epoxy. The head-plate was laser cut from 1.5 mm thick 304L stainless steel with a brushed finish to facilitate dental cement adhesion. The head-plate was attached using both M1.4 screws and dental cement after the animals fully recovered from the cranial window surgery. Further details can be found in Appendix 1.

Cranial window surgery and COMBO window installation

Mice were anesthetized with a subcutaneous injection of a fentanyl (0.05 mg/kg), midazolam (5 mg/kg), and medetomidine (0.5 mg/kg) (FMM) cocktail. Mice were then secured using a bite bar and placed on top of a temperature controller (Supertech) to maintain a body temperature of 37°C. Hydration gel (Bayer, Bepanthen) was placed on the eyes to prevent dryness during surgery. A dental drill was then used to cut a large cranial window into the skull, which generally spanned from bregma +2.25 mm AP to bregma -4.00 mm AP and the full width of the dorsal skull. The bone island was removed and the dura was left intact. The pre-prepared COMBO window was then attached to the remaining bone using cyanoacrylate glue (Pattex) and sealed with dental cement (Super-Bond). After surgery, anesthesia was reversed with a subcutaneous injection of a naloxone (1.2 mg/kg), flumazenil (0.5 mg/kg), and atipamezole (2.5 mg/kg) cocktail. Carprofen (20 mg/kg) was injected subcutaneously for post-surgical analgesia. After seven days of recovery, animals were again anesthetized with FMM as previously described and the head-plate was attached to the COMBO window. After at least three more days of recovery animals began habituation to the experimenter, the behavioral setups, and tasks.

Virus injection and fiber implantation

For animals used in optogenetic experiments, virus injection and fiber implantation was performed prior to the craniotomy in the same surgery. Animals were anesthetized using the FMM cocktail previously described and secured in a stereotaxic frame (Stoelting). Mice were then injected

bilaterally with 500 nl of AAV-CaMKIIa-ChR2-EYFP (Addgene, #50469, 2.3 x 10^13 particles per ml) in the secondary motor cortex (AP: 2.90 mm, DV: 0.80 mm, ML: +/- 1.0 mm at an angle of 30 degrees from the vertical). Custom-made optic fibers (200 µm core, 0.22 NA) were then implanted 200 µm above the injection site along the same trajectory. A minimal amount of cyanoacrylate glue was applied to the fibers and skull for stabilization while paying special attention to not cover the area intended for the cranial window. Then, the craniotomy was performed and the "anterior" COMBO window installed as previously described. In accordance with the smaller opening of the COMBO designs meant to accommodate optic fibers, these cranial windows generally spanned from bregma -1.50 mm AP to bregma -4.00 mm AP. The fiber compartment was then also filled with dental cement to ensure robust attachment to the skull.

Optogenetic stimulation

A 200 µm diameter optical fiber (Doric Lenses Inc.) was connected to a 473 nm laser (LaserGlow) and to each of the implanted fibers. The laser power was adjusted to 5-6 mW at the tip of each fiber. For experiments with simultaneous fUS and videography, a single stimulation run consisted of a block design with 90 sec of baseline, followed by 10 sec of optical stimulation (20 Hz, 10 ms pulse width) delivered every 90 sec. Similarly, for optogenetic stimulation during electrophysiological recordings, a block design with 9 sec of baseline, followed by 1 sec of optical stimulation (5 Hz, 10 ms pulse width) was delivered every 9 sec. Stimulation was triggered using a pre-programmed pulse generator (Doric, OTPG_8), which was synchronized with the fUS acquisition software, videographic recordings and/or electrophysiological recordings, respectively.

Visual stimulation

For visual stimulation, full-field drifting gratings were presented with a spatial frequency of 20° and velocity of 10°/sec on a standard 61 cm computer monitor (Dell, U2415b) using the PsychoPy toolbox. The monitor was placed 18 cm in front of the mouse. We employed a block design consisting of 12 sec of gray background followed by 12 sec of drifting gratings (one of four cardinal directions). Each direction was repeated three times, resulting in twelve stimulation blocks per recording run.

fUS acquisition

fUS imaging data was acquired using a 32 x 32 channel matrix probe (15 MHz, 1024 total elements, spatial resolution: 220 x 280 x 175 μm^3, Vermon) attached to a Vantage 256 (Verasonics, Inc.) and controlled by a custom vfUSI acquisition module (AUTC) [22]. At the beginning of each imaging session the matrix probe was positioned to encompass the full width and length of the cranial window using a three-way translation stage. Briefly, a single compound ultrasound image was generated from the summation of the reconstructed echoes of plane wave emissions at -4.5, -3, -1.5, 0, 1.5, 3, 4.5 degrees. A single power Doppler image was created from the incoherent average of 160 compound ultrasound images acquired at a pulse repetition frequency of 400 Hz. Clutter filtering was performed in real time whereby the compound ultrasound stack was decomposed using singular value decomposition and the first 20% of singular vectors were removed. This procedure produced a single power Doppler image every ~500 ms.

fUS preprocessing

The fUS time series was first registered to the reference mouse brain atlas from the Allen Brain Institute. To do so, 100 fUS frames from a single recording session were first averaged together to create a higher resolution power Doppler image. This high-quality image was then manually registered (rotation and translation only) to the atlas using anatomical landmarks for a mouse-specific transformation matrix. This transformation matrix was then applied to data from other sessions from the same mouse. fUS time series were then preprocessed using custom MATLAB scripts on a voxel-by-voxel basis. First, data was temporally interpolated to obtain a constant frame rate of 2 Hz. Next, the relative change in power Doppler signal was calculated by first subtracting the baseline signal (mean of the 11 frames for data in Figure 3 or 70 frames for data in Figure 5 before each stimulus) from each time point and then dividing the result by the baseline signal. Subsequently, to remove slow drifts, the data was filtered with a 5th-order highpass Butterworth filter with a cutoff frequency of 0.056 Hz. Lastly, to remove unspecified movement artifacts during awake experiments, we removed the first principal component from the spatial-temporal decomposition of the entire time series. In addition, we removed motion artifact time points by interpolating those that were above a voxel-specific threshold, defined as the median + absolute deviation of signal * 4.44).

fUS activation

For voxel-wise analysis, preprocessed fUS data was analyzed with a general linear model (GLM) analysis on a voxel-wise basis. First, a temporal smoothing of four frames was applied to the time series of each voxel, which was then fitted with a GLM using the MATLAB glmfit.m function. Model regressors included the optogenetic or visual stimulation block stimuli, after being convolved with a single-gamma hemodynamic response function. For each voxel a one-sample t-test on the resulting T-scores from different sessions was performed and voxels with FDR-corrected p-value below 0.05 are displayed. The statistics were calculated across sessions since few animals were used for the presented proof-of-concept experiments.

For region-based analysis in Figures 3 and S6, preprocessed and trial averaged whole-brain data was segmented into individual brain regions. Anatomical regions from the Allen reference brain atlas were condensed into 100 brain regions and used to segment the fUS time series by averaging the information from all voxels within a single region. To define active brain regions in response to visual and optogenetic stimulation, the correlation coefficient between the stimulus timing and the fUS-signal of a brain-region was calculated and a one-sample t-test on these correlation coefficients for each region was performed. All regions with an FDR-corrected p-value below 0.05 (0.001 for Figure S6c) were determined active. To visualize brain-wide activity across time in Supplementary Video 4, voxels and time points with low activity ($\Delta I/I < 1.75\%$) or high mean baseline activity ($\Delta I/I > 5\%$) were masked.

Two-photon microscopy acquisition

Ca^{2+} imaging was performed with a two-photon moveable objective microscope (Sutter Instruments) using a 20x objective (NA 1.0, Zeiss) and ScanImage software. GCaMP was excited at 940 nm using a Ti:sapphire laser (Mai Tai, Spectra Physics) and emission was detected using

a GaAsP photomultiplier tube (Hamamatsu) through a bandpass emission filter (525/70 nm). To minimize photobleaching, laser intensity was adjusted for each field of view. Images were acquired on behaving mice that were head-fixed under the microscope on a custom-built running wheel. Time series data were acquired with a field of view of 525.17 μm^2 x 525.17 μm^2 (512 x 512 pixels) at 30 Hz for 90 seconds, 200-300 µm below the pial surface in the retrosplenial (RSC) and secondary motor cortices (M2), respectively.

Two-photon microscopy analysis

All raw fluorescence images were preprocessed with Suite2p [36], which included image registration, cell detection and time series extraction. All labeled cells were confirmed or removed based on visual inspection of both the image and time series. For each recording, the time series of all cells was spatiotemporally decomposed using singular value decomposition. The first right singular vector, representing the time series of the first principal component, was smoothed with a 0.5 sec sliding window and was correlated with the locomotion trace. The same was performed on the time series of each individual cell.

Electrophysiology recordings

32-channel silicon probes (Cambridge NeuroTech, type H10b) with a 32-channel headstage (Intan technologies, C3324) were connected via a SPI interface cable (Intan technologies, C3216) to an USB interface board (Intan technologies, C3100). Data was recorded at 20 kHz using RHX software. Mice were anesthetized using the same FMM cocktail as previously described and head-fixed in a holding tube. The head of the mouse was aligned in all three axes to the coordinate system of the probe manipulator. Bilateral openings in the COMBO window film above the midbrain (AP: 4.00 mm, ML: 1.00) were created using a drill, and the probe was lowered into the midbrain at a speed of 2 µm/s. Data was acquired at three different depths (DV: -2.20 mm, -2.60 mm and -3.60 mm below the brain surface) in both hemispheres during separate recordings. Concurrent optogenetic stimulation and electrophysiological recordings were performed 10 min after reaching the desired depth. CM-DiI (Thermo Fisher, CellTracker) was applied to the probe prior to brain insertion to allow post-hoc confirmation of the recording site.

Electrophysiology analysis

Electrophysiological recordings were analyzed using kilosort3 [47], and spike sorting results were manually curated using the phy software (https://github.com/cortex-lab/phy). Only units with stable responses across the duration of the session and high kilosort quality scores were included in subsequent analysis. To obtain continuous firing rate estimates, single unit responses were binned with a bin size of 1 ms and convolved with a gaussian kernel with a standard deviation of 10 ms. For visualization in Figure 5 the firing rate of each cell was smoothed with a 70 ms window, and then trial-averaged and z-scored to the 4.5 sec before stimulus onset. The Gramm toolbox [48] was used to visualize raster plots in Figure 5. For cell response-type classification in Figure S6f the trial averaged continuous firing rate of each cell was correlated to different stimulus windows. Cells that positively correlated ($r > 0.2$) with the stimulus timing were defined ON cells, cells that negatively correlated with the stimulus timing ($r < -0.2$) deactivated cells and cells that correlated positively ($r > 0.2$) with a window from stimulus offset to 800ms after stimulus offset were named OFF cells.

Open-field foraging task

Control mice and those with a COMBO window were handled by the experimenter for at least 2 days prior to the open field. Mice were placed in a 40 cm x 40 cm square arena (Stoelting) with opaque gray walls. A single diffuse LED light source was placed above the arena to ensure uniform lighting, and food pellets were scattered throughout the arena to promote exploration. A 1.3 megapixel monochromatic camera (Flir, BFS-U3-13Y3M-C) was positioned above the arena to capture the full field and recorded the animals' behavior for 10 min each at 20 Hz. Females were tested before males and the arena was cleaned between each animal. Mouse activity tracking was performed in Matlab using open-source code provided by Zhang et al. [49] as well as custom scripts. Mouse position data was downsampled by a factor of 3 and smoothed using a 0.5 sec window before calculating the distance and speed between time points. Tortuosity was calculated as described in Zong et al. [27]. Briefly, the tortuosity of a given window (1.2 sec sliding window) was calculated as the ratio between the actual distance traveled by the mouse and the length of the straight path between two points. Then the median tortuosity of all time points where the mouse was running (speed threshold defined as the average of the 75th percentile of running speeds in control animals) was calculated.

Facial videography

Videographic recordings were acquired using a 1.3 megapixel monochromatic camera (Flir, BFS-U3-13Y3M-C) either in the dark (two-photon imaging, fUS + visual stimulation) or in the presence of a small LED light (facial expressions, fUS + optogenetic stimulation). Videos for the facial imaging and during optogenetics experiments were acquired at 20 Hz, while those during two-photon calcium recordings were acquired at 30 Hz. One camera was always positioned such that the frame contained the full face, from ear to snout, and in some cases also the front two paws. In some experiments a second camera was positioned with a field of view that captured the entire body of the animal. In general, two or three 875 mm IR LED arrays (Kemo Electronic M120) were pointed at the face to enable recordings in the dark. A 720 nm (Hoya, R72 E49) filter was attached to the camera to remove non-IR light. Videographic recordings were initiated using a TTL trigger that was aligned to the start of two-photon or fUS imaging acquisition.

Habituation to head fixation

Prior to a recording session, all animals were gradually habituated to a head-fixed context. During the first 1-2 days of handling by the experimenter, animals were allowed to explore the behavior rig. Over the next 5+ days, the animals were head-fixed with the duration of fixation increasing on each subsequent day starting from 10 min and eventually reaching 60 min. Additional experimental components such as a computer screen or water spout were gradually introduced over the course of the habituation procedure.

Head-fixed behavioral analysis

During two-photon videographic recordings, the front paws were tracked using DeepLabCut [50]. The resulting x and y position time series were used to create a distance measurement at every time point that represented the movement of the paw(s) relative to the previous frame. A locomotion time series was then created by averaging the movement time series of the left and

right paw, which was then smoothed with a 0.5 sec (15 frame) sliding window. Videographic recordings during optogenetic stimulation were analyzed using FaceMap [51]. The motion energy was extracted from regions-of-interest (ROIs) placed over the whisker pad of the animal and of the wheel (without any body part visible), to obtain a proxy of whisking and locomotion, respectively. Whisking and locomotion time-series were z-scored on a trial-by-trial basis to the 40 sec before stimulus onset. To define trials with and without optogenetically-induced locomotion in Figure S6, a threshold was applied to the average z-score during the period between stimulus onset and 10 sec after stimulus offset (>2 with locomotion, <2 without locomotion).

Facial expression analysis

Facial expression analysis was performed in accordance with the methods described in Dolensek et al. [31]. After being habituated to a running wheel and water spout, animals were each administered five trials (2 sec, 120 sec inter-stimulus interval) of 20% sucrose and 10 mM quinine in subsequent runs. Similarly, baseline periods were defined as 2 sec long intervals before any stimulus was presented and in which the animal exhibited no locomotion and minimal orofacial movement. HOG descriptors for each video frame were extracted with the following parameters: 32 pixels per cell, 1 cell per block, 8 orientation bins.

Histogram of oriented gradient (HOG) facial analysis was performed in Matlab using custom scripts. Emotion prototypes were created for each mouse individually. Prior to HOG extraction, facial images were cropped to include only the face, ear and whiskers of the mouse. An ROI containing the spout was also marked so that corresponding indices could be removed from all future HOG analyses. A neutral prototype was first created by averaging the HOG vectors from the previously described baseline periods. The HOG time series from stimulus runs were then correlated (Pearson's correlation coefficient) with this neutral prototype. The HOG vectors of the ten least correlated time points during sucrose/quinine delivery were averaged to create the pleasure/disgust prototypes, respectively. To examine the neutral, pleasure and disgust responses during different conditions, a time-resolved correlation coefficient was computed between each of the three emotion prototypes and the HOG vectors of the sucrose and quinine stimulus runs. This resulted in a neutral, pleasure and disgust similarity time series for each of the sucrose and quinine runs, from which periods around stimulus/condition onset were extracted and visualized.

Immunohistochemistry

A subset of animals (N = 6 COMBO, N = 5 control) were anesthetized with a ketamine (120 mg/kg) and xylazine (16 mg/kg) cocktail and transcardially perfused with 0.1 M phosphate-buffered saline (PBS), followed by 4% paraformaldehyde (PFA) in PBS. The brain was extracted and fixed in 4% PFA overnight at 4 °C, followed by submersion in 20% sucrose in 0.1 M PBS for up to one week at 4 °C.

50 µm thick coronal brain sections were acquired using a vibratome (Leica) and stored in cryoprotection solution at -20 °C for up to one week prior to staining. For GFAP staining, sections were transferred to 0.1 M PBS for 30 minutes, followed by washing in 0.1 M PBS containing 0.5% Triton X-100 for 10 minutes. Afterward, the sections were incubated in blocking solution,

containing 10% blocking agent (Normal Serum Block, CAT# 927502, Biolegend) in 0.1 M PBS with 0.5% Triton X-100 for 2 hours. Subsequently, the sections were transferred to blocking solution containing 1:1000 primary antibody rabbit Polyclonal anti-GFAP (PA5-16291, ThermoFisher Scientific) for 24 hours at 4 °C. Sections were washed four times in 0.1 M PBS with 0.5% Triton X-100 for 5-10 minutes each and then incubated in blocking solution containing 1:400 secondary antibody donkey Polyclonal anti-rabbit Alexa Fluor Plus 488 (A32790, ThermoFisher Scientific) for 2.5 hours. Sections were washed four more times in 0.1 M PBS with 0.5% Triton X-100 for 5-10 minutes and then mounted on glass slides using Fluoromount-G with DAPI (Thermo Fisher Scientific). Individual sections were imaged using a slide scanner (Olympus) using a 10x objective.

For virus expression and electrode track identification, brain sections were sliced, stored and mounted as described above, but without any additional staining procedure. Individual sections were imaged using a slide scanner (Olympus) using a 4x objective.

GFAP fluorescence quantification

To quantify and compare GFAP fluorescence throughout the area spanned by the window, we imaged three sections per brain corresponding to approximately bregma +2.0 mm AP, bregma -1.0 mm AP, and bregma -3.0 mm AP. Similar slices were imaged and quantified in both control animals and those with a COMBO window. GFAP immunofluorescence was then quantified using custom Matlab scripts. In each slice, 6 regions-of-interest (ROIs) with a diameter of 250 μm were manually selected uniformly across the cortex, focusing on superficial layers and the pial surface. The GFAP fluorescence was taken as the average intensity within each ROI.

AUTHOR CONTRIBUTIONS:

Conceptualization: BJE, DS, EM; Data Curation: BJE, DS, PW; Formal Analysis: BJE, DS; Funding Acquisition: BJE, DS, NG, TF, EM; Investigation: BJE, DS, PW, BJ, BS, AR; Methodology: BJE, DS, PW, BJ, NG, TF, EM; Project Administration: BJE, EM, Resources: NG, TF, EM; Software: BJE, DS, EM; Supervision: BJE, NG, TF, EM; Validation: BJE, DS, PW, EM; Visualization: BJE, DS, EM; Writing - Original Draft: BJE, DS, EM: Writing - Review & Editing: BJE, DS, PW, TF, EM

A tabular display of these contributions is in **Supplementary Table 3**.

DATA AVAILABILITY:

All data needed to evaluate the conclusions in the paper are present in the paper or the Supplementary Materials. All relevant COMBO window files, raw fUS and two-photon data, along with the corresponding videographic recordings will be available at 10.5281/zenodo.8223630. Additional data and software supporting the findings of this study are available from the corresponding authors upon reasonable request.

ACKNOWLEDGMENTS:

This work was funded by the Max-Planck Society and the Deutsche Forschungsgemeinschaft (DFG, German Research Foundation) under Germany's Excellence Strategy - EXC 2067/1-390729940). B.J.E. was supported by the European Molecular Biology Organization Postdoctoral Fellowship no. ALTF 449-2020. D.S. was supported by the Swiss National Science Foundation (SNSF) Early Postdoc.Mobility no. 194957, SNSF Postdoc.Mobility no. 211087 and Deutsche Forschungsgemeinschaft Walter-Benjamin Programm (Stelle) no. SI 2831/1-1. We thank Julia Kuhl for her help on figure illustrations and our colleagues from the Macé, Frank, and Gogolla labs for their comments on the manuscript.

DISCLOSURES:

The authors have nothing to disclose.

REFERENCES:

1. Lin, A. *et al.* Imaging whole-brain activity to understand behaviour. *Nat. Rev. Phys.* **4**, 292–305 (2022).
2. Urai, A. E., Doiron, B., Leifer, A. M. & Churchland, A. K. Large-scale neural recordings call for new insights to link brain and behavior. *Nat. Neurosci.* **25**, 11–19 (2022).
3. Aimon, S. *et al.* Fast near-whole–brain imaging in adult Drosophila during responses to stimuli and behavior. *PLOS Biol.* **17**, e2006732 (2019).
4. Portugues, R., Feierstein, C. E., Engert, F. & Orger, M. B. Whole-Brain Activity Maps Reveal Stereotyped, Distributed Networks for Visuomotor Behavior. *Neuron* **81**, 1328–1343 (2014).
5. Koch, C. *et al.* Next-generation brain observatories. *Neuron* **110**, 3661–3666 (2022).
6. de Vries, S. E. J., Siegle, J. H. & Koch, C. Sharing Neurophysiology Data from the Allen Brain Observatory: Lessons Learned. Preprint at https://doi.org/10.48550/arXiv.2212.08638 (2022).
7. The International Brain Laboratory *et al.* Standardized and reproducible measurement of decision-making in mice. *eLife* **10**, e63711 (2021).
8. Macé, É. *et al.* Whole-Brain Functional Ultrasound Imaging Reveals Brain Modules for Visuomotor Integration. *Neuron* **100**, 1241-1251.e7 (2018).
9. Sans-Dublanc, A. *et al.* Optogenetic fUSI for brain-wide mapping of neural activity mediating collicular-dependent behaviors. *Neuron* **109**, 1888-1905.e10 (2021).
10. Isshiki, M. & Okabe, S. Evaluation of cranial window types for in vivo two-photon imaging of brain microstructures. *Microscopy* **63**, 53–63 (2014).
11. Kim, G., Rabut, C., Ling, B., Shapiro, M. & Daraio, C. *Microscale acoustic metamaterials as conformal sonotransparent skull prostheses*. https://www.researchsquare.com/article/rs-2743580/v1 (2023) doi:10.21203/rs.3.rs-2743580/v1.
12. Rabut, C. *et al.* A window to the brain: ultrasound imaging of human neural activity through a permanent acoustic window. *BioRxiv Prepr. Serv. Biol.* 2023.06.14.544094 (2023) doi:10.1101/2023.06.14.544094.

13. Holtmaat, A. *et al.* Long-term, high-resolution imaging in the mouse neocortex through a chronic cranial window. *Nat. Protoc.* **4**, 1128–1144 (2009).

14. Trachtenberg, J. T. *et al.* Long-term in vivo imaging of experience-dependent synaptic plasticity in adult cortex. *Nature* **420**, 788–794 (2002).

15. Cramer, S. W. *et al.* Through the looking glass: A review of cranial window technology for optical access to the brain. *J. Neurosci. Methods* **354**, 109100 (2021).

16. Kim, T. H. *et al.* Long-Term Optical Access to an Estimated One Million Neurons in the Live Mouse Cortex. *Cell Rep.* **17**, 3385–3394 (2016).

17. Donaldson, P. D. *et al.* Polymer Skulls With Integrated Transparent Electrode Arrays for Cortex-Wide Opto-Electrophysiological Recordings. *Adv. Healthc. Mater.* **11**, 2200626 (2022).

18. Ghanbari, L. *et al.* Cortex-wide neural interfacing via transparent polymer skulls. *Nat. Commun.* **10**, 1500 (2019).

19. Aydin, A.-K. *et al.* Transfer functions linking neural calcium to single voxel functional ultrasound signal. *Nat. Commun.* **11**, 2954 (2020).

20. Boido, D. *et al.* Mesoscopic and microscopic imaging of sensory responses in the same animal. *Nat. Commun.* **10**, 1110 (2019).

21. Kılıç, K. *et al.* Chronic Imaging of Mouse Brain: From Optical Systems to Functional Ultrasound. *Curr. Protoc. Neurosci.* **93**, (2020).

22. Brunner, C. *et al.* A Platform for Brain-wide Volumetric Functional Ultrasound Imaging and Analysis of Circuit Dynamics in Awake Mice. *Neuron* (2020) doi:10.1016/j.neuron.2020.09.020.

23. Brunner, C. *et al.* Whole-brain functional ultrasound imaging in awake head-fixed mice. *Nat. Protoc.* **16**, 3547–3571 (2021).

24. Hattori, R. & Komiyama, T. Longitudinal two-photon calcium imaging with ultra-large cranial window for head-fixed mice. *STAR Protoc.* **3**, (2022).

25. Eng, L. F. Glial fibrillary acidic protein (GFAP): the major protein of glial intermediate filaments in differentiated astrocytes. *J. Neuroimmunol.* **8**, 203–214 (1985).

26. Hobbiesiefken, U., Mieske, P., Lewejohann, L. & Diederich, K. Evaluation of different types of enrichment - their usage and effect on home cage behavior in female mice. *PLOS ONE* **16**, e0261876 (2021).

27. Zong, W. *et al.* Large-scale two-photon calcium imaging in freely moving mice. *Cell* **185**, 1240-1256.e30 (2022).

28. Musall, S., Kaufman, M. T., Juavinett, A. L., Gluf, S. & Churchland, A. K. Single-trial neural dynamics are dominated by richly varied movements. *Nat. Neurosci.* **22**, 1677–1686 (2019).

29. Stringer, C. *et al.* Spontaneous behaviors drive multidimensional, brainwide activity. *Science* **364**, 255 (2019).

30. Zhao, Z. *et al.* Ultraflexible electrode arrays for months-long high-density electrophysiological mapping of thousands of neurons in rodents. *Nat. Biomed. Eng.* **7**, 520–532 (2022).

31. Dolensek, N., Gehrlach, D. A., Klein, A. S. & Gogolla, N. Facial expressions of emotion states and their neuronal correlates in mice. *Science* **368**, 89–94 (2020).

32. Macé, E. *et al.* Functional ultrasound imaging of the brain. *Nat. Methods* **8**, 662–664 (2011).

33. Dinh, T. N. A., Jung, W. B., Shim, H.-J. & Kim, S.-G. Characteristics of fMRI responses to visual stimulation in anesthetized vs. awake mice. *NeuroImage* **226**, 117542 (2021).

34. Peters, A. J., Fabre, J. M. J., Steinmetz, N. A., Harris, K. D. & Carandini, M. Striatal activity topographically reflects cortical activity. *Nature* **591**, 420–425 (2021).

35. Chen, T.-W. *et al.* Ultrasensitive fluorescent proteins for imaging neuronal activity. *Nature* **499**, 295–300 (2013).

36. Pachitariu, M. *et al.* Suite2p: beyond 10,000 neurons with standard two-photon microscopy. (2016) doi:10.1101/061507.

37. Kong, L., Little, J. P. & Cui, M. Motion quantification during multi-photon functional imaging in behaving animals. *Biomed. Opt. Express* **7**, 3686–3695 (2016).

38. Villette, V. *et al.* Ultrafast Two-Photon Imaging of a High-Gain Voltage Indicator in Awake Behaving Mice. *Cell* **179**, 1590-1608.e23 (2019).

39. Steinmetz, N. A., Zatka-Haas, P., Carandini, M. & Harris, K. D. Distributed coding of choice, action and engagement across the mouse brain. *Nature* **576**, 266–273 (2019).

40. Magno, L. A. V. *et al.* Optogenetic Stimulation of the M2 Cortex Reverts Motor Dysfunction in a Mouse Model of Parkinson's Disease. *J. Neurosci.* **39**, 3234–3248 (2019).

41. Billeh, Y. N. *et al.* Effects of Chronic Sleep Restriction during Early Adolescence on the Adult Pattern of Connectivity of Mouse Secondary Motor Cortex. *eNeuro* **3**, ENEURO.0053-16.2016 (2016).

42. Oh, S. W. *et al.* A mesoscale connectome of the mouse brain. *Nature* **508**, 207–214 (2014).

43. Edelman, B. J. *et al.* High-sensitivity detection of optogenetically-induced neural activity with functional ultrasound imaging. *NeuroImage* **242**, 118434 (2021).

44. Tournissac, M. *et al.* Cranial window for longitudinal and multimodal imaging of the whole mouse cortex. *https://doi.org/10.1117/1.NPh.9.3.031921* **9**, 031921 (2022).

45. Bergel, A., Deffieux, T., Demené, C., Tanter, M. & Cohen, I. Local hippocampal fast gamma rhythms precede brain-wide hyperemic patterns during spontaneous rodent REM sleep. *Nat. Commun.* **9**, 5364 (2018).

46. Bergel, A. *et al.* Adaptive modulation of brain hemodynamics across stereotyped running episodes. *Nat. Commun.* **11**, 6193 (2020).

47. Pachitariu, M., Sridhar, S. & Stringer, C. Solving the spike sorting problem with Kilosort. 2023.01.07.523036 Preprint at https://doi.org/10.1101/2023.01.07.523036 (2023).

48. Morel, P. Gramm: grammar of graphics plotting in Matlab. *J. Open Source Softw.* **3**, 568 (2018).

49. Zhang, C., Li, H. & Han, R. An open-source video tracking system for mouse locomotor activity analysis. *BMC Res. Notes* **13**, 1–6 (2020).

50. Mathis, A. *et al.* DeepLabCut: markerless pose estimation of user-defined body parts with deep learning. *Nat. Neurosci.* **21**, 1281–1289 (2018).

51. Syeda, A. *et al.* Facemap: a framework for modeling neural activity based on orofacial

tracking. 2022.11.03.515121 (2022) doi:10.1101/2022.11.03.515121.

Supplementary Materials

The COMBO window: A chronic cranial implant for multiscale circuit interrogation in mice

Bradley Jay Edelman[*,#], Dominique Siegenthaler[*], Paulina Wanken, Bethan Jenkins, Bianca Schmid, Andrea Ressle, Nadine Gogolla, Thomas Frank, Emilie Macé[#]

*These authors contributed equally to this work
Correspondence to: bradley_edelman@psych.mpg.de, emilie.mace@bi.mpg.de

Files:

Supplementary File 1: COMBO_cup.stl
Supplementary File 2: COMBO_flat.stl
Supplementary File 3: COMBO_lateral.stl
Supplementary File 4: COMBO_posterior.stl
Supplementary File 5: COMBO_anterior.stl
Supplementary File 6: COMBO_Q1.stl
Supplementary File 7: COMBO_Q2.stl
Supplementary File 8: COMBO_Q3.stl
Supplementary File 9: COMBO_Q4.stl
Supplementary File 10: Head_plate.dwg
Supplementary File 11: Head_plate_holder.sldprt
Supplementary File 12: Head_plate_holder_top.dwg
Supplementary File 13: Head_plate_holder_bottom.dwg
Supplementary File 14: Brain_mold.stl

Videos:

Supplementary Video 1: Facial videography during a trial of sucrose delivery
Supplementary Video 2: Facial videography during a trial of quinine delivery
Supplementary Video 3: Brain-wide fUS activity in awake mice in response to visual stimulation
Supplementary Video 4: Facial videography and two-photon imaging in the retrosplenial cortex during locomotion

Figures:

Supplementary Figure 1: Head fixation part details
Supplementary Figure 2: COMBO window assembly and installation instructions
Supplementary Figure 3: Sporadic GFAP fluorescence was observed in mice implanted with the COMBO window
Supplementary Figure 4: Behavioral effects are consistent across sex and individuals
Supplementary Figure 5: The COMBO window enables chronic brain-wide acquisition of fUS data
Supplementary Figure 6: The COMBO window facilitates longitudinal experiments to interrogate neural circuits underlying behavior.

Tables:

Supplementary Table 1: Open field foraging task statistical analysis
Supplementary Table 2: Facial expression statistical analysis
Supplementary Table 3: Author Contributions

Appendix:

Appendix 1: COMBO window preparation and installation protocol

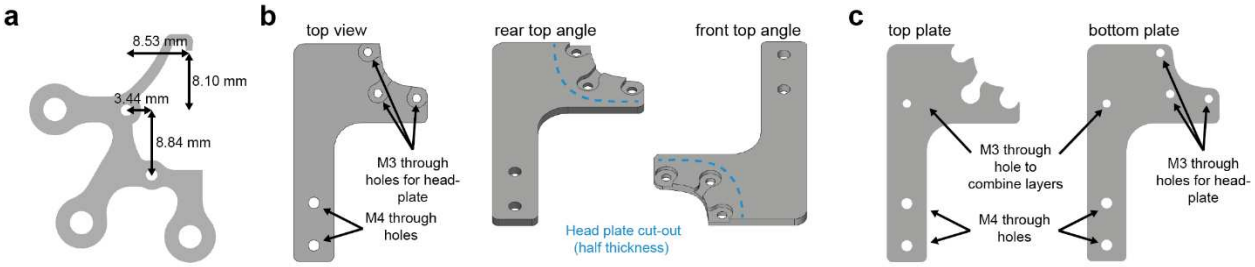

Supplementary Figure 1: Head fixation part details

a Computer-aided design of the standard COMBO window head-plate (Supplementary File 10). The head-plate attaches to the implant via two M1.4 through holes at the side and rear, as well as a peg in the front. Other custom head plate designs with the same features and relative distances can also be used for head fixation. **b** The standard head-plate holder design (Supplementary File 11) consists of a single metal plate with the head plate outline cut halfway through the total thickness. Threaded M3 screws are welded into the head-plate holes and grinded flush with the underside of the plate. M4 through holes allow for attachment to other commercial or custom parts for further stabilization. It is recommended that a machine shop helps with the fabrication of this part. **c** An alternative head-plate holder design consists of a top and bottom plate (Supplementary Files 12-13) that can each be laser cut and joined together with no custom fabrication. M3 screws can be used to secure the two layers together, and M4 screws to attach the head-plate holder to other commercial or custom parts. Additional M3 screws can be attached via the underside of the holder using glue/epoxy.

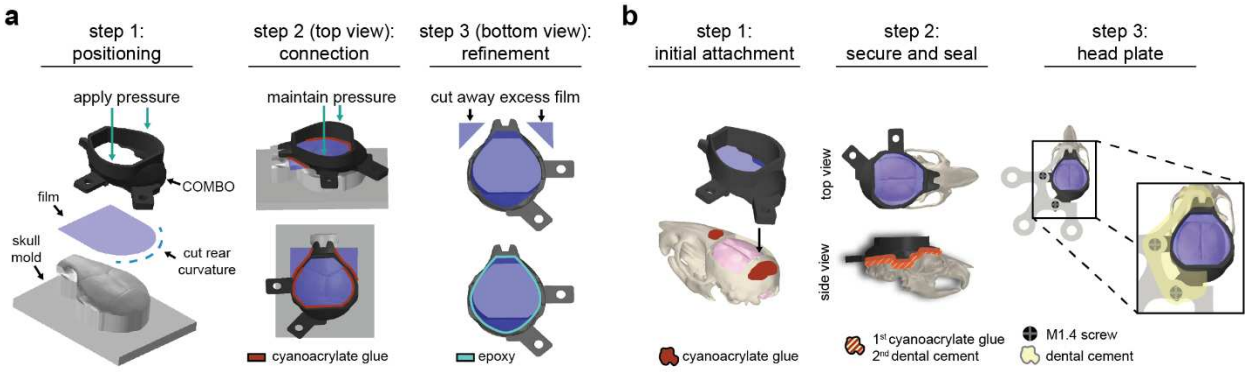

Supplementary Figure 2: COMBO window assembly and installation instructions

a Three-step diagram of the preparation of the COMBO window. Using the skull mold (Supplementary File 14) is recommended but not required for proper assembly. **b** Three-step diagram of the installation of the COMBO window after a cranial window has been created. The head plate can be installed at the same time as Steps 1-2 or at a later date. Detailed methods for both of the procedures are provided in Appendix 1.

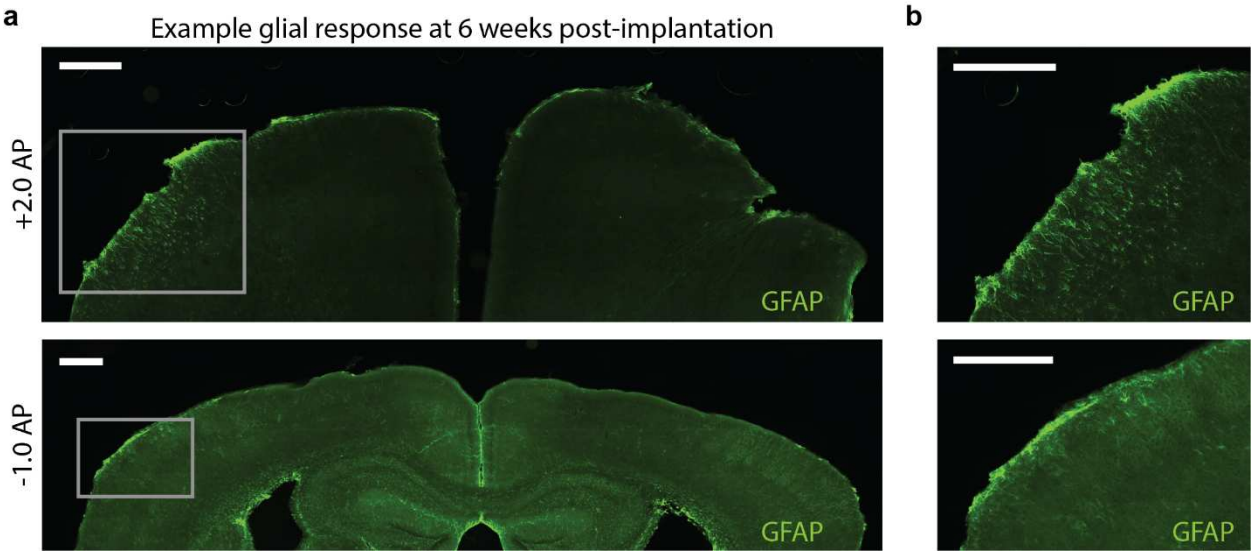

Supplementary Figure 3: Sporadic GFAP fluorescence was observed in mice implanted with the COMBO window

a Glial fibrillary acidic protein (GFAP) fluorescence in two example slices (top: bregma +2.0 mm AP, bottom: bregma -1.0 mm AP) of mice at 6 weeks after being implanted with the COMBO window. In both images, a localized increase of GFAP fluorescence can be seen in the left hemisphere. **b** Zoomed-in images of the elevated GFAP signal indicate that the immune response was found mostly in fibers located at or near the pial surface. Scale bars represent 500 μm.

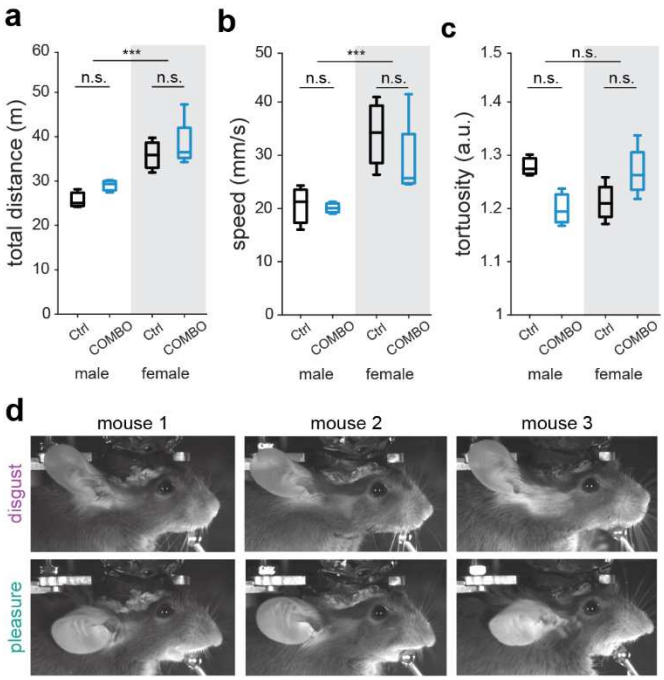

Supplementary Figure 4: Behavioral effects are consistent across sex and individuals

a-c The total distance (**a**), speed (**b**), and tortuosity (**c**) of control and COMBO window mice separated into male (n = 3) and females (n = 4). Boxplots represent the median (center line), 25th and 75th percentiles (lower and upper box), and the 1st and 99th percentile (whiskers). Two-way ANOVA on ranks with main effects of sex and cranial window. Main effect of sex: *** $p < 0.001$. Post hoc pairwise t-tests, Bonferroni corrected: n.s. $p > 0.05$. **d** Example prototypical disgust and pleasure facial expressions exhibited by three animals with a “cup” version of the COMBO window installed. Key features of the elicited disgust face include a flaring back of ear and an upturned snout, and of the elicited pleasure face include the forward movement of the ear and a downturned snout.

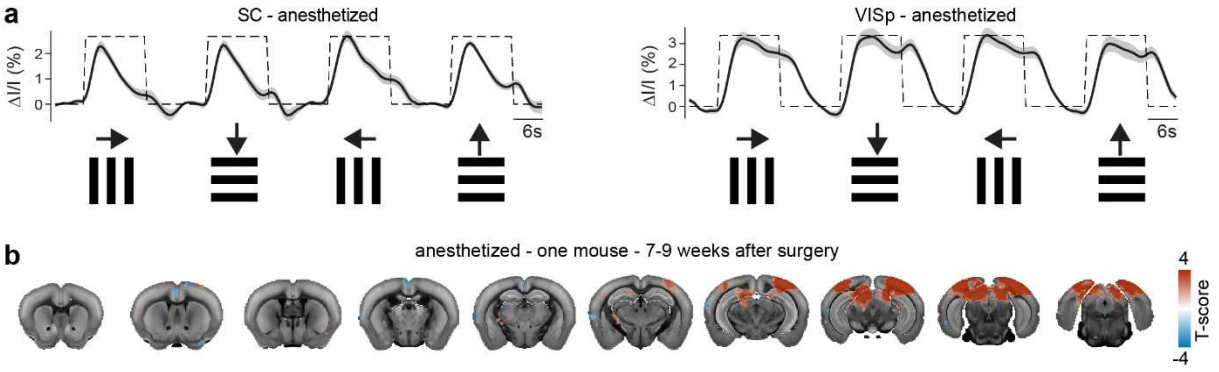

Supplementary Figure 5: The COMBO window enables chronic brain-wide acquisition of fUS data

a fUS signal in the superior colliculi (SC) and primary visual cortex (VIS) of anesthetized mice covaries in response to drifting gratings in all four cardinal directions (N = 5 mice, n = 32 sessions). The dark black line and light gray shaded area represent the mean ± s.e.m. across sessions. **b** GLM results from 8 sessions of a single mouse recorded 7-9 weeks after surgery overlayed on the Allen Brain Atlas. Only voxels with an average T-score > 2 are displayed.

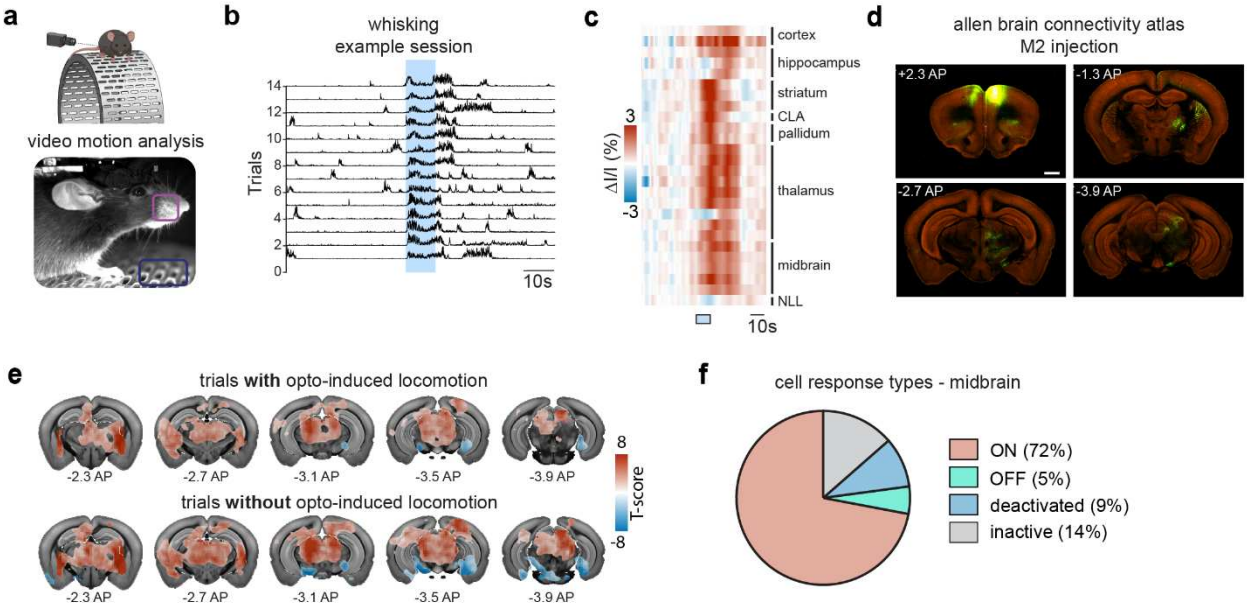

Supplementary Figure 6: The COMBO window facilitates longitudinal experiments to interrogate neural circuits underlying behavior

a Facial videography was used to monitor animal behavior on a running wheel. Regions-of-interest (ROIs) placed over the whisker pad (violet) and wheel (green) were utilized to capture whisking activity and locomotion, respectively, induced by optogenetic stimulation of the secondary motor cortex (M2). **b** Consecutive trials from the same example session as in Figure 5c showing a robust and reliable increase in whisking in response to optogenetic activation of M2. Each trial was z-scored to a pre-stimulus baseline and rescaled between 0 and 1 for visualization purposes. **c** Region-wise segmented results of the optogenetically-induced fUS activity. Regions are sorted by brain area, and only significantly modulated (correlation between stimulus timing and fUS signal) regions are included (significantly different from zero across sessions, $p < 0.001$, FDR-corrected). **d** Example coronal slices from the Allen Brain Connectivity Atlas (connectivity.brain-map.org/projection/experiment/287995889). AAV tracings after injection into the M2 (1) show widespread axonal projections from M2 to the striatum, the thalamus and the midbrain (2 - 4). Scale bar represents 1 mm. **e** GLM analysis of fUS data in response to optogenetic stimulation of M2 (N = 2 mice, n = 12 sessions). In contrast to Figure 5e, here the trials were separated according to strong or weak locomotor response (see methods for threshold definition) to optogenetic stimulation. Only the voxels with T-scores significantly different from zero across sessions ($p < 0.05$, FDR-corrected) are shown. **f** Pie chart showing the proportion of different cell response types observed in the midbrain (see methods for cell response type definition).

Supplementary Table 1: Open field foraging task statistical analysis

Parameter	Statistical Test	Comparison	Post Hoc Test	P-value
Total Distance	Two-way ANOVA on ranks CW vs Ctrl F(1,13) = 1.93, p = 0.19 Male vs Female F(1,13) = 34.05, ***p = 0.002	COMBO vs Ctrl (Male only)	Bonferroni	p = 1.00
		COMBO vs Ctrl (Female only)	Bonferroni	p = 1.00
Speed	Two-way ANOVA on ranks CW vs Ctrl F(1,13) = 0.75, p = 0.41 Male vs Female F(1,13) = 31.21, ***p = 0.002	COMBO vs Ctrl (Male only)	Bonferroni	p = 1.00
		COMBO vs Ctrl (Female only)	Bonferroni	p = 1.00
Tortuosity	Two-way ANOVA on ranks CW vs Ctrl F(1,13) = 1.27, p = 0.29 Male vs Female F(1,13) = 0.03, p = 0.86	COMBO vs Ctrl (Male only)	Bonferroni	p = 0.06
		COMBO vs Ctrl (Female only)	Bonferroni	p = 0.48

Supplementary Table 2: Facial expression statistical analysis

Parameter	Statistical Test	Comparison	P-value
Disgust	Wilcoxon rank sum test	Quinine vs Neutral	p = 0.0001
		Sucrose vs Neutral	p = 1.00
Pleasure	Wilcoxon rank sum test	Quinine vs Neutral	p = 0.92
		Sucrose vs Neutral	p = 0.0011

Supplementary Table 3: Author Contributions

	BJE	DS	PW	BJ	BS	AR	NG	TF	EM
Conceptualization	X	X							X
Data Curation	X	X	X						
Formal Analysis	X	X							
Funding Acquisition	X	X					X	X	X
Investigation	X	X	X	X	X	X			
Methodology	X	X	X	X			X	X	X
Project Administration	X								X
Resources							X	X	X
Software	X	X							X
Supervision	X						X	X	X
Validation	X	X	X						X
Visualization	X	X							X
Writing - Original Draft	X	X							X
Writing - Review & Editing	X	X	X					X	X

Appendix 1: COMBO window preparation and installation protocol

1. COMBO Window Preparation

1.1. Download and print one of the COMBO window files (**Supplementary Files S1-9**) and the Brain_mold.stl (**Supplementary File 14)** using a 3D printer.

NOTE: If the 3D printer utilizes supports when printing, they should be placed on the top of the implant frame and on the bottom of the skull mold to ensure smooth contact surfaces between these two parts. The supports should be cut away and the contact points sanded smooth.

1.2. Thread the two holes of the implant frame using a M1.4 tap. Due to animal safety and physical difficulty, these holes should not be threaded after implantation.

1.3. Cut a square of film (0.125 mm thickness) slightly bigger than the implant frame. Cut a round edge on one side of the film to fit the curvature at the posterior end of the implant frame (**Supplementary Figure 2a, step 1**).

1.4. Place the film on the bottom mold (round part at the back) with the implant frame on top. Apply pressure at the edges of the implant frame downward onto the mold. Try to minimize buckling and ensure that there are no gaps between the film and the implant frame (**Supplementary Figure 2a, step 1**). Multiple attempts to achieve proper positioning may be needed.

1.5. While maintaining pressure, apply a conservative amount of tissue adhesive (low-viscosity cyanoacrylate glue) to the interior rim of the implant frame to attach the film. It is also recommended to apply super glue (high-viscosity cyanoacrylate glue) to the exterior of the frame where any excess film protrudes (**Supplementary Figure 2a, step 2**). After a few minutes (to allow the glue to dry), if these steps have been performed correctly, the implant frame and the film can be removed from the mold together. Other types of glue can also be placed on various interior/exterior edges of the frame according to what is easiest for the user.

NOTE: Avoid covering the film with glue as this can affect the transparency of the window.

1.6. Apply a layer of epoxy to the border of the interface between the film and the implant frame (**Supplementary Figure 2a, step 3**).

1.7. Let the epoxy dry overnight and remove the excess film using a scalpel on the following day. Then, file the hardened epoxy as close to the implant frame as possible (**Supplementary Figure 2a, step 3**). Repeat steps 1.6 – 1.7 until the film is fully secured to the implant frame with no gaps, and is flush with the surface.

NOTE: Before implant installation, ensure that the implant is thoroughly cleaned using 100% ethanol.

1.8. Download the Head_plate.dwg file (**Supplementary File 10**) and laser cut this shape from 1.5 mm stainless steel. A brushed finish will increase the grip of the dental cement.

2. COMBO Window Installation

2.1. Cranial Window Surgery

2.1.1 Prepare the animal for surgery according to locally approved animal licenses and secure the animal's head using a bite bar or stereotaxic frame.

2.1.2. Using sterile scissors cut a 2 cm midline incision through the scalp and periosteum to expose the skull. This incision should reach from just behind the ears to the middle of the eyes.

2.1.3. Detach the periosteum using a cotton-tipped applicator. Then, detach the temporalis and trapezius muscles on the sides and rear of the skull, respectively, using scissors or forceps. Try to maximize the surface area of exposed skull to allow firm attachment of the implant in later steps. Ensure that the skull surface is dry using cotton tipped applicators (use 0.3% H2O2 if necessary).

NOTE: Avoid damaging vessels behind the eyes and at the rear of the skull when detaching the muscles. Damaging such vessels can cause large bleeds and will reduce the animal's chance of survival.

2.1.4. Push the muscles down and secure them to the skull in place using tissue adhesive. Make sure that no gaps remain and that, as mentioned above, as much of the skull stays exposed as possible. Clean debris from the skull surface with a wet cotton-tipped applicator and dry with compressed air.

2.1.5. Set hand drill to ~5000 rotations per minute and mark an outline of the craniotomy on the skull by drilling superficially. Briefly, the extent of the craniotomy can extend the full width of the skull and from the rostral rhinal vein (anterior) to the transverse sinus (posterior) (or even further to the end of the cerebellum). Additional details regarding steps 2.1.5. – 2.1.7. can be found in Brunner et al. 2021 and Hattori et al. 2022.

2.1.6. Continue to deepen the outline by repeatedly moving the drill over the initial groove until the bone island is "floating" on top of the brain. Use compressed air to gently blow away bone debris as needed. Occasionally apply cool saline to the skull to prevent overheating.

2.1.7. To remove the skull, use forceps (e.g. 90 degree) to lift the anterior edge of the bone towards the posterior end. For this, cover the skull with buffer or saline and gently lift the bone island little by little until the soft tissue connections have fully detached from the dura and vessels. The dura should be left intact.

NOTE: There are strong soft tissue connections between the skull and dura along the superior sagittal sinus. Removing the skull too quickly and under too dry of conditions can rip the SSS and cause a potentially fatal bleed. This step can take up to 15 minutes or more for correct detachment without major bleeding.

2.1.8. After removal of the bone, clean the edges of the craniotomy and ensure that the residual bone surface is dry before proceeding with the next steps. Keep the dura moist at all times.

2.2 Implant Attachment and Sealing

2.2.1. Rinse the ethanol-cleaned implant with saline and let it dry on a paper towel.

2.2.2. Place a small amount of super glue on the skull, anterior and posterior to the cranial window. Gently place the implant on top of the cranial window, ensuring that there is secure contact with the areas covered with super glue (**Supplementary Figure 2b, step 1**). The implant should hug the sides and the rear of the skull in this step.

NOTE: Some of the film may make direct contact with the dura during this step, but full contact is not necessary at this point. If sealed properly, the window will fill up with cerebrospinal fluid within a few days (**Figure 1b**).

2.2.3. Once the implant feels secure, place additional super glue in the gaps between the implant and the skull to fully secure and seal the implant to the skull (**Supplementary Figure 2b, step 2**).

NOTE: There is generally less skull exposed at the anterior parts of the head, and it can therefore be difficult to properly seal this section (especially around the eyes). If these sections are not properly sealed, dental cement can easily fall through this gap and onto the brain surface in step 2.2.4.

2.2.4. Prepare dental cement according to the manufacturer's instructions and apply generously around the circumference of the implant and skull (on top of the glue) (**Supplementary Figure 2b, step 2**). Ensure that there are no gaps between the implant and skull. Contact with the sutured skin will largely prevent the animal from opening wounds.

2.2.5. Attach the head-plate to the implant with two M1.4 screws (**Supplementary Figure 2b, step 3**). Prepare additional dental cement and apply to the two screws and front peg to ensure that the head-plate is locked in place on the implant. Additional cement can be placed in the gap between the head-plate and implant for a firmer connection (**Supplementary Figure 2b, step 3**). This step can also be performed in a second surgery after recovery from the craniotomy and implant installation.

2.2.6. Apply silicone (e.g. Kwik-Cast silicone sealant) on top of the film to protect it until imaging.

2.2.7. Reverse the anesthesia and provide post-operative care according to locally approved animal licenses for the required number of days. When the animal is returned to its home cage, it is strongly recommended to remove any overhead gratings in the home cage to avoid interference with the implant/head-plate, and place additional feed on the floor of the cage.

3. Head Fixation and Imaging

3.1. We propose two assembly methods of the head fixation system for securing the mouse to the experimental setup. For the first (preferred) design, download the Head_fixation.sldprt file (**Supplementary File S11**) and manufacture the shape from 2 mm stainless steel from an external provider or workshop. Alternatively, the Head_plate_holder_top.dwg and Head_plate_holder_bottom.dwg files can be used together to construct the same design (**Supplementary Files S12-13**). This approach has the advantage of being compatible with laser cutting. Each part should be laser cut from 1 mm stainless steel and secured together via the rear mounting holes (M4 through holes). In either case, thread the fixation holes (M3 through holes) with an M3 tap and feed M3 screws (with low profile heads) upward through each. Alternatively, the M3 screws can be permanently secured with epoxy or M3 studs can be welded in place. The head fixation should be secured in the behavioral setup prior to the start of habituation.

3.2. Animals should be handled for three days for 10 - 15 min per day prior to being trained on a particular behavioral setup. On the first day of habituation to the setup, allow the mouse to first explore as performed previously. After 5 - 10 minutes, position the animal into alignment with the head fixation screws. Gently lift the head-plate with a pair of forceps onto the pins while supporting the body of the animal with the other hand. Tighten M3 nuts on top of the pins to secure the head-plate, first by hand and then using a socket driver. The duration of a habituation session should increase each day for at least five days.

3.3. On days in which imaging takes place, remove the silicone window protection, and wash the surface of the film with saline and dry with a cotton-tipped applicator. After imaging is complete, it is recommended that the silicone window protection be replaced (while the animal is still head-fixed) until the next imaging session.